BCURA Contract B74

Final Report : October 2004 - September 2007

The Properties and Combustion Characteristics of Coal-derived Fuels for Industrial Gas Turbine Applications

Birute Bunkute and Barrie Moss

University Project Manager:

Professor JB Moss
Combustion Centre, School of Engineering
Cranfield University
Bedford MK43 0AL

Tel: 01234 754635 ; Fax: 01234 752452 ; email; j.b.moss@cranfield.ac.uk

Industrial Supervisor:

Mr. G. Kelsall
Aero- and Thermodynamics
Alstom Power Ltd
Newbold Road
Rugby CV21 2NH

Tel: 01788 531739 ; email; greg.kelsall@power.alstom.com

September 2007

Executive Summary

The combined cycle gas turbine burning premium gaseous fuels, predominantly natural gas, has had a substantial impact in recent years on the efficiency, cleanliness and cost of power generation in the UK. Future resource projections and strategic considerations, however, have prompted renewed interest also in advanced coal technology - seeking thereby to exploit a long-lived fossil fuel resource – in addition to the combustion of renewables such as the fuels derived from bio-mass. Currently, natural gas-fuelled gas turbines provide a particularly challenging performance benchmark for thermal power generation based on coal burning. However, integrated gasification combined cycle (IGCC) plant hold the prospect of coal utilisation that also capitalises on such technology.

Syngas fuels from coal (or oil) gasification typically comprise mixtures of H_2, CO and N_2 but may also include smaller concentrations of hydrocarbons, CO_2 and H_2O. The specific composition will depend on the source fuel and the detail of the gasification process – whether , for example, the gasification employs air or oxygen . A key feature of the necessary combustion technology is therefore that it be robust in the face of generally greater variability in the fuel specification.

The objectives of the present study are therefore threefold:
(a) to establish a database of combustion properties – in particular , laminar burning velocity and ignition delay – for syngas fuel mixtures representative of gasified coal at conditions relevant to the gas turbine,
(b) to combine measurement and numerical simulation such that a robust methodology can be identified which both validates results obtained under common conditions and also permits their prediction for mixtures and conditions that are not accessible experimentally,
(c) to demonstrate the application of such data to the flowfield simulation of a representative gas turbine combustor.
The key features of the approach adopted and their outcomes are summarised below.

The work was divided into two parts that were performed in parallel: chemical kinetics simulations of laminar burning velocities, critical strain rate to extinction and autoignition delay for a wide range of fuel mixtures; and measurements of laminar burning velocity based on Schlieren photography for four syngas mixtures with fuel mixture compositions of 67%CO/33%H_2; 1.5%CO/28.5%H_2/70%N_2, 50%CO/50%H_2 and 57%H_2/43%N_2 for a range of reactant preheat temperatures and pressures. Experiments were performed for these mixtures using two burner geometries: a convergent nozzle (exit diameter 10mm) and a long (50 diameters length) straight pipe of 5mm in diameter. The burner was fitted with a water cooling jacket to minimise rim heating effects and mounted in a pressure casing.

The laminar burning velocity was observed to increase substantially with increase in reactant preheat temperature for all mixtures. There is generally good agreement between experimental results and numerical predictions for temperatures up to 400K; the discrepancy is less than 10% for mixtures with 67%CO/33%H_2 and 50%CO/50%H_2 compositions. The explanation for the observed discrepancies appears to lie in some uncertainty in the reactant preheat temperature measurement. Thermocouple measurements at the burner exit are impractical and can only be made in the absence of the flame. During the test campaign at higher reactant temperatures it was observed, however, that the burner exit temperature was strongly dependent on only the reactant mass flow and therefore temperature calibration based on this mass flow was performed and adopted for purposes of reactant preheat temperature estimation. Experiments for all gases were performed at elevated pressures in order to investigate their effect on laminar burning velocity. We observed that only very lean laminar flames could be adequately stabilised and only for pressures up to 5bar. It was not possible to obtain high

pressure data for richer flames because the Re number of the flow in the tube approached a value of 2000 and so enters the transitional regime from laminar to turbulent flow.

Unlike the corresponding numerical simulations, these experiments suggest that pressure has only a small effect on laminar burning velocities at very lean equivalence ratios. This trend is not predicted in simulations using GRI Mech 3.0 and would seem to imply shortcomings in the reaction mechanism for very lean flames at high pressures. Alternatively, it is possible that the discrepancy lies in the flame area inferred from the Schlieren images. If the flame shape is distorted, the area may be significantly under-estimated, resulting in an exaggerated laminar burning velocity. Lean flames at higher pressures did show increasing evidence of cellular disturbance.

Numerical simulations were carried out to accumulate additional laminar burning velocity data for artificial neural network (ANN) training. CO_2 and H_2O diluents were added to the $CO/H_2/N_2$ fuel mixtures to enlarge the database. Simulations of ignition delay time using a perfectly stirred reactor were also performed for the range of CO/H_2 mixtures. The effects of temperature, pressure, equivalence ratio and fuel mixture composition on autoignition delay were investigated. Given the comparative insensitivity to equivalence ratio only stoichiometric mixtures were investigated in detail. Temperature has the most significant effect on ignition delay; with increase in temperature, the ignition delay time drops exponentially, reflecting the increase in mixture reactivity.

CFD simulations of the reacting flow within a representative combustor geometry have been performed in order to demonstrate the utilization of the combustion properties data obtained from the chemical kinetic simulations and the ANNs. Their implementation in a partially premixed combustion model that incorporates the effects of chemistry through a burning velocity closure is shown to be simple and robust.

Numerical simulation that is both flexible in its application and sufficiently reliable to reduce the need for extensive combustor testing and development is critical to addressing the design demands for increased gas turbine fuel flexibility. The present comparisons between prediction and experiment give confidence in the detailed chemical kinetic mechanisms available for syngas mixtures and the opportunities for expanding such data sets to less experimentally accessible conditions using artificial neural networks. The data and methodologies will assist both gas turbine manufacturers and operators of generating equipment in evaluating the consequences of introducing lower calorific value syngas into the fuel inventory.

Table of contents

Figures

Tables

1. Introduction

Background

The combined cycle gas turbine burning premium gaseous fuels, predominantly natural gas, has had a substantial impact in recent years on the efficiency, cleanliness and cost of power generation in the UK. Future resource projections and strategic considerations, however, have prompted renewed interest also in advanced coal technology - seeking thereby to exploit a long-lived fossil fuel resource – in addition to the combustion of renewables such as the fuels derived from bio-mass. Currently, natural gas-fuelled gas turbines provide a particularly challenging performance benchmark for thermal power generation based on coal burning. However, integrated gasification combined cycle (IGCC) plant hold the prospect of coal utilisation that also capitalises on such technology.

Syngas fuels from coal (or oil) gasification typically comprise mixtures of H_2, CO and N_2 but may also include smaller concentrations of hydrocarbons, CO_2 and H_2O. The specific composition will depend on the source fuel and the detail of the gasification process. A key feature of the necessary combustion technology is therefore that it be robust in the face of generally greater variability in the fuel specification.

The low levels of NO_X emitted by current gas turbines burning natural gas, typically less than 10 ppm in many applications, have been achieved with highly refined strategies for fuel-air mixture preparation based on a combination of empiricism and numerical simulation. Stable, lean burning combustion systems present a considerable design challenge, even for premium fuels. The starting point for similar combustor developments in relation to hydrogen / carbon monoxide mixtures, coupled with some variability in composition, temperature and water content is much less secure. Differences in calorific value of the fuel, reflecting the level of inert ballast, combined with those in stoichiometry, flammability and flame stability introduce changes to combustion characteristics that must be accommodated through design. Unlike natural gas (or methane) that has attracted a wide range of combustion applications over very many years and for which an extensive combustion database has been developed, gaseous fuel mixtures of the kind derived from coal have not been widely investigated.

Figure 1 illustrates some of the key features of typical syngas compositions derived from differing gasification processes and feedstocks. The data are distinguished by the broad characterisation of the gasifier in respect of the method of feed coal transport. The nitrogen content will largely depend on whether the oxidiser employed, in conjunction with steam, is air or oxygen. Working temperature and residence time will also play significant roles in determining hydrocarbon content and fuel calorific value.

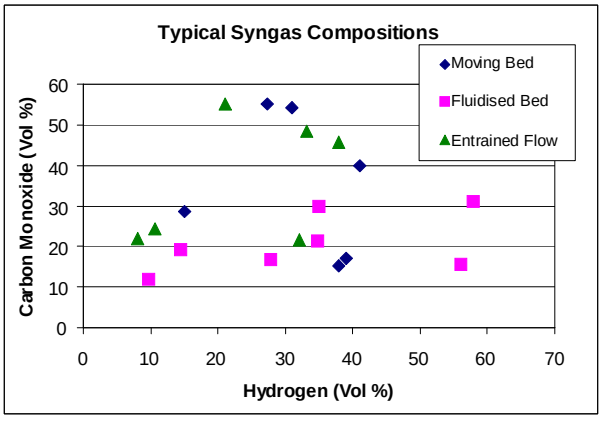

a)

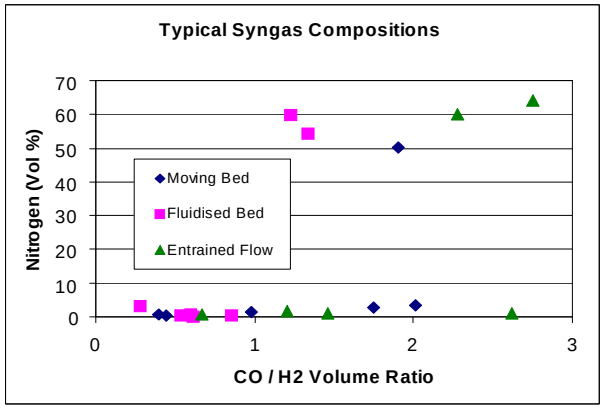

b)

Figure 1: Typical syngas compositions

Given the variability in fuel gas composition, numerical simulation provides valuable flexibility in extending restricted measurement sets of combustion properties and in subsequently assessing their implications for combustor design under widely varying input conditions.

1.2 Research Objectives

The specific objectives of the research are threefold:

(d) To establish a database of combustion properties – notably, laminar burning velocity and ignition delay – for syngas fuel mixtures representative of gasified coal at conditions relevant to the gas turbine.

(e) To combine measurement and numerical simulation such that a robust methodology can be identified which both validates results obtained under common conditions and permits their prediction for mixtures and conditions that are not accessible experimentally.

(f) To demonstrate their application in a representative gas turbine combustor simulation.

1.3 Programme

Direct measurements of laminar burning velocity, based on Schlieren imaging, have been made for representative H_2 / CO / N_2 fuel mixtures burning at predominantly lean equivalence ratios in the range 0.4 – 1.4 for initial reactant temperatures up to 600K and a working pressures of ~ 5bar.

These data have been computed using one-dimensional flame codes incorporating detailed chemical reaction mechanisms. Comparisons between measurement and computation have then guided additional experiments and extensions of the data to higher pressures and reactant temperatures. The individual computations with comprehensive chemistry are time consuming and have therefore, in turn, been used to train artificial neural networks permitting the more rapid development of the complete database. Additional work (not explicitly identified in the original proposal) in the form of complementary calculations of ignition delay for these mixtures are also reported, incorporating an assessment of their enhanced sensitivity to details of the chemical scheme. This data has implications for the stability of the combustion process under high inlet temperature conditions that is relevant to both future practical application and to the electrical mixture heating in the experimental study undertaken here.

In the final phase, the syngas burning velocity data have been incorporated in CFD simulations of a generic combustor for which there are data in the open literature – albeit only when fuelled by natural gas. This affords a demonstration of the data implementation and comparison with a premium fuel.

2. Experimentation

2.1 Rig Design

There are three broad strategies in regard to flame configuration for laminar burning velocity measurement: stationary flames stabilized on burner ports; stationary flames in stagnating or impingement flows; and freely propagating flames within confined volumes (or bombs). None is ideal and each impose restrictions – relevant to the gas turbine operating regime – in terms of reactant temperature and working pressure. In the present study we have adopted the ported flame configuration, capitalising on an existing pressure casing with good optical access.

The basic layout is illustrated in Figure 2. Two burners have been investigated: a convergent nozzle of 10mm exit diameter, machined in stainless steel and incorporating a 4:1 contraction, and a straight cylindrical tube of internal diameter 5mm, 50 diameters in length. The former gives an essentially uniform exit velocity profile with only a thin wall boundary layer whilst the latter produces fully developed laminar pipe flow. The hydrodynamic strain developed by the velocity profile in the reactant mixture is different in the two cases and comparisons between the two sets of results introduce an opportunity to examine the influence of such strain on both the measured burning velocity and the stability of lean rim-stabilised laminar flames. The reactant mixture can be electrically preheated, together with the wire -wrapped burner tube, to temperatures approaching those of autoignition. Controlling conditions at the burner rim is generally more problematic, however, and a number of variants have been investigated with a view to extending the stable burning regime. In the presence of the flame, heat is transferred to the rim – principally by conduction since the flame is barely luminous. Locally the metal temperature can exceed the planned level of preheat and therefore, at low heating rates, some rim cooling can also be introduced through a water jacket extending over the last 10 mm of the cylindrical burner.

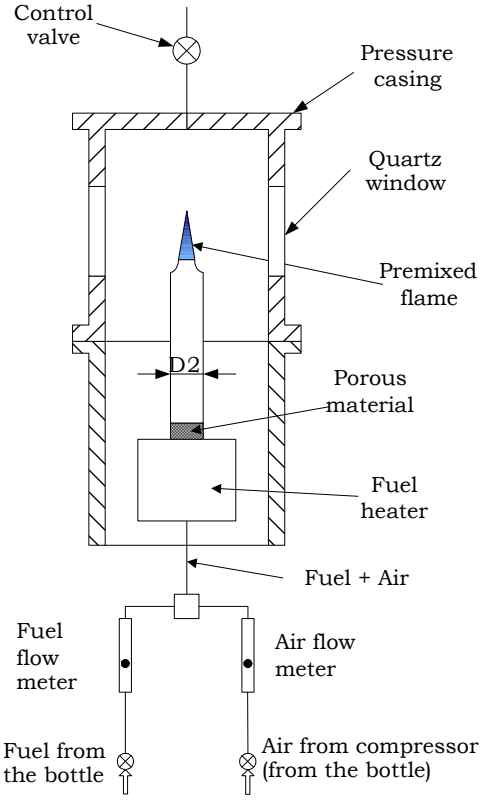

Figure 2: Schematic of the burner configuration, casing and reactant supply

The burners are mounted within a stainless steel pressure vessel of internal diameter 300mm, fitted with optical quality quartz windows of 75mm diameter that provide line-of-sight access for the Schlieren system. Additional smaller ports provide access for probes and a heated coil igniter. The vessel can be pressurised using a variable area exhaust orifice up to a casing limit of 15 bar. As later results show, it has not proved possible in practice to satisfactorily stabilise flames beyond ~7 bar. Whilst reactant heating provides some relief from the effects of increasing chamber pressure on pipe Reynolds number, through the increased viscosity, this is limited. Since the reduction in laminar burning velocity with increased pressure (and hence reactant flow velocity) is comparatively modest, the influence of density predominates and transitional Reynolds numbers ~ 2000 are readily attained.

2.2 Methodology

The flame luminosity is very low but the leading edge of the reaction zone has been imaged using a conventional Z-configuration Schlieren system [1] incorporating two 100 mm diameter mirrors with focal lengths of 1m. Edge detection software is used to determine the flame boundary and the flame area is inferred from considerations of symmetry (cf. Figure 3). The conical flame boundary is divided into segments and the area of each elemental frustrum is calculated and summed. The area averaged laminar burning velocity, S_L, is then computed from the measured mass flow rate, $\dot{m}$, the reactant mixture density, ρ_u and the total flame area, ΣA_i in the form:

$$S_L = \frac{\dot{m}}{\rho_u \Sigma A_i}$$

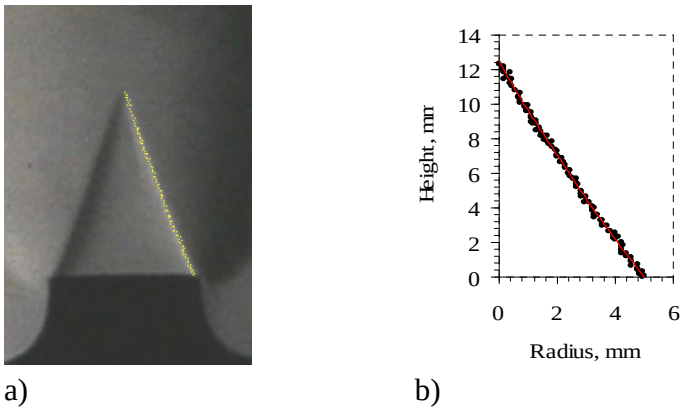

a) b)

Figure 3: Schlieren image edge detection

Flame curvature is greater for the 5mm plain tube and varies with reactant mixture.

Ignition of the flame within the chamber is achieved using an electrically heated coil. Once a stable flame is established, the two-dimensional traverse on which the burner is mounted is used to displace the flame relative to the stationary igniter. At some conditions, the regime of stable burning – free from the cellular distortion that is discussed later – is extremely narrow and it proved necessary to tailor the equivalence ratio and mass flow rate to the visual nature of the flame. This is then reflected in the scatter on some of the data points in composition space.

2.3 Test Conditions

Three fuel mixtures have been investigated, spanning a range of calorific values, fuel-air stoichiometric ratios and burning velocities. The three fuels – subsequently distinguished as Flames A, B and C – are identified in Table 1. The equivalent natural gas characteristics are included solely for comparison purposes though it should be noted that the laminar burning velocity for natural gas under ambient conditions at ~ 40 cm/s is broadly comparable with the nitrogen diluted mixture of Flame A.

Table 1: Fuel composition

Fuel Composition	28.5%H_2/1.5%CO/70%N_2	33%H_2/67%CO	50%H_2/50%CO	Natural Gas
Calorific Value (LCV) [MJ/kg]	3.6	13.8	17.5	48.2
Stoichiometric Air-fuel Ratio (mass)	1.0	3.5	4.6	16.5

A very limited data set was obtained for a stream blended fuel mixture of 60%H_2/40% N_2 which is briefly reported later.
The three fuel mixtures are each taken from commercially prepared cylinders.

The burning velocity data are restricted to a maximum reactant temperature of 600K and 7 bar pressure, with the experimentally accessible range of fuel-air mixture equivalence ratios decreasing with increasing temperature and pressure. The limiting pipe Reynolds number drives the experimental conditions to ever leaner mixtures – lower burning velocities and hence lower reactant velocities – as the working pressure is increased. The maximum working temperature is limited by uncertainty over the peak gas temperatures that might be attained within the electrical heater and the associated autoignition hazard. System heat losses required that temperatures measured within the heater exceeded those at the burner exit by at least 100^0C.

3. Numerical Simulations

3.1 Laminar Burning Velocity

The variable nature of the fuel composition adds weight to the role played by numerical simulation in assessing combustion performance. In parallel with the experimental investigation of laminar burning velocity for a prescribed set of fuel mixtures, the base cases have also been simulated numerically, together with extensions to some operating conditions not accessible to measurement and more complex fuel mixtures. These latter include components additional to H_2, CO and N_2, introducing both diluents (H_2O, CO_2) and the hydrocarbon, CH_4.

The simulations have been performed using the 1-D counter-flow configuration in the CHEMKIN suite [2] and the freely propagating flame model in the open source code CANTERA [3]. In both cases, the chemical reaction mechanism employed is GRI-Mech.3.0 [4]. Though developed primarily for methane combustion, the mechanism comprising 325 reversible reactions and 53 chemical species incorporates a detailed description of H_2 and CO oxidation. No significant differences were observed between the two codes on common test cases and the choice between them was largely a matter of availability and ease of use.

The simulations of those mixtures and conditions common to the experimental measurement campaign are reported, together with the measured data, in Section 4 of this report. The results of a broader range of simulations, including temperatures up to 800K and pressures up to 15bar are presented in Appendix A.

3.2 Flame Stretch

In addition to its dependence on state properties – composition, temperature and pressure – the burning velocity is also influenced by the hydrodynamic field in which combustion takes place. Whilst the open laminar Bunsen flame imposes a fairly benign strain field, the practical application in the gas turbine involves both high levels of flow velocity and intense turbulent fluctuations. Although the comparisons between numerical prediction and laminar flame measurement are therefore performed at low strain rates, data at strain rates up to flame extinction are needed for the simulation of turbulent premixed burning. The computations in the OPPDIF component of CHEMKIN are therefore made over a range of strain rates – by varying the counter flowing stream velocities – and the zero strain rate value is determined by extrapolation.

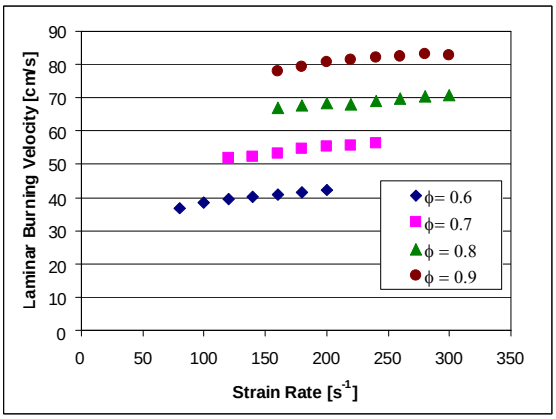

Figure 4: Computed variation of laminar burning velocity with strain rate for the 33%H_2/67% CO fuel burning in air over a range of equivalence ratios (ϕ)

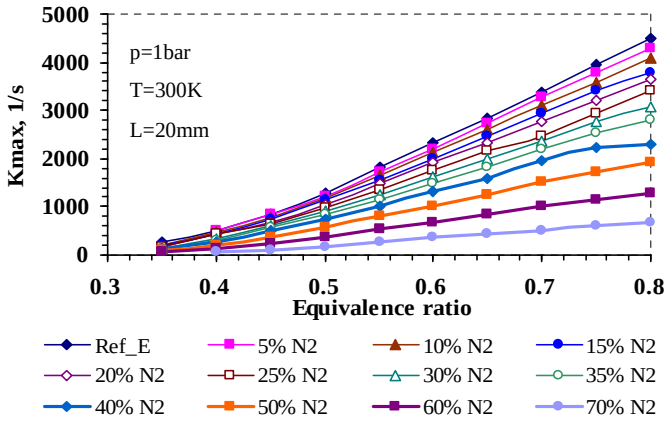

Figure 5: Extinction strain rates for CO/H_2 fuel mixtures with N_2 addition burning in air for a range of equivalence ratios

The burning velocity is observed to increase with strain rate, albeit modestly by comparison with the effects of changes in state properties, whilst the sensitivity of the critical strain rate at extinction to changes in equivalence ratio is predicted to decrease very significantly with increasing nitrogen dilution.

3.3 Artificial Neural Networks

In order to provide a flexible tool for the calculation of burning velocities of CO/H_2/Diluents fuel mixtures over a wide range of fuel compositions, mixture equivalence ratios and operating conditions, the detailed chemical kinetic calculations have been used to train an artificial neural network (ANN) [5] . The ANN simulations have been performed in the MATLAB environment using the Neural Networks Toolbox. For a representative test data set, the best ANN built on 2000 data points, and incorporating 8 input neurons, 1 hidden layer with 11 neurons and one output neuron, yielded an R^2 correlation of 0.9992. The ANN was validated against several literature sources, including the 50%CO/50%H_2 data at 700K of Natarajan et al [6] and the experimental and numerical burning velocity data for a fuel mixture of 49.24%H_2/29.41%CO/ 1.35%N_2 at a preheat temperature of 673K from Zajadatz et al [7]. The comparisons between the source data and their ANN simulations are illustrated in fig.6.

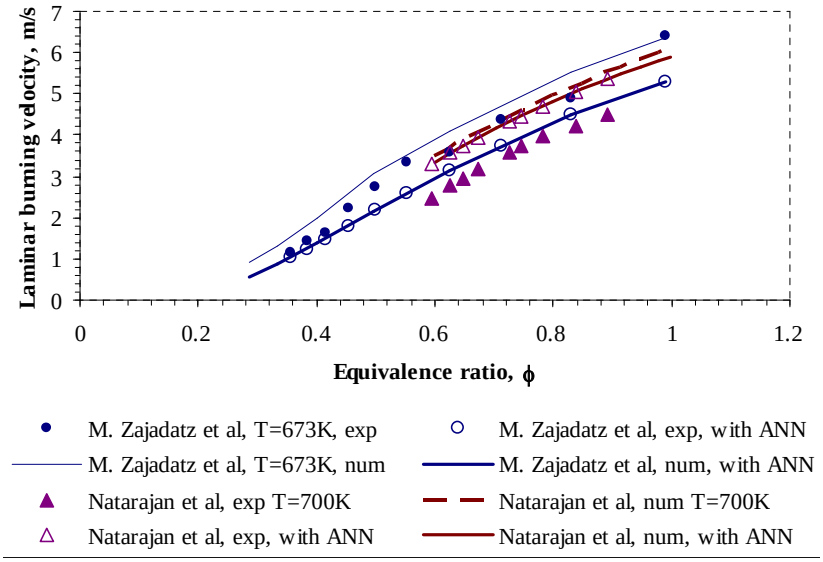

Figure 6: Comparison between ANN predictions of laminar burning velocity and data from measurement and calculation reported in the open literature

More detail on the ANN and, in particular, a summary of the system of describing equations are presented in Appendix B.

3.4 Combustor CFD

Incorporation into CFD prediction of the burning velocity data obtained in this study is illustrated in respect of a typical partially-premixed combustion model of the kind employed, for example, in the commercial FLUENT code. Mathematical closure of the chemical source term in the equation for mean reaction progress is achieved through an estimate of turbulent burning velocity, U_{turb}, for the local fuel-air mixture that is related to both the laminar burning velocity – representing the influence of chemistry- and the local computed turbulence field. For example, [8]

$$U_{turb} = A\, u'^{3/4} U_{lam}^{1/2} \alpha^{-1/4} \ell_{turb}^{1/4}$$

where A is a model constant, u' is the rms turbulent velocity fluctuation, U_{lam} is the laminar burning velocity, α is the thermal diffusivity and ℓ_{turb} is the integral turbulence length scale. The model incorporates the influence of hydrodynamic strain on the laminar burning velocity through the locally computed turbulence properties.

Illustrative comparisons of the application of this partially premixed model to the combustor geometry investigated in the EU sponsored programme PRECCINSTA are presented in Appendix C.

4. Results and Discussion

Experiments with a number of CO/H_2 – air mixtures exhibited distorted flame shapes that made the assumption regarding symmetry about the burner axis unreliable. Some illustrative flame shapes will be briefly described later in this section. Given that the objective of the present study was to measure laminar burning velocities of syngas – air mixtures as a function of equivalence ratio, temperature and pressure, the range of experimentally accessible mixture equivalence ratios is limited by the onset of such disturbances. The area-averaged laminar burning velocity measurements cited in this report are therefore restricted to continuous and smooth flame structures.

For the mixtures 67%CO/33%H_2, 50%CO/50%H_2 and 57%H_2/43%N_2 burning at ambient pressure the flames formed smooth inner cones of uniform luminosity. Only a small number of very lean flames with equivalence ratio below 0.55 attained polyhedral shapes.

For the mixture 1.5%CO/28.5%H_2/70%N_2 , flame cones at equivalence ratios above 0.78 were also smooth.

4.1 Experimental Data at Ambient Conditions

Fuel Mixture with 67%CO/33%H_2

The burning velocities were found to vary from 0.3 m/s to 0.8 m/s for the measured equivalence ratio range, see Figure 7. These data were obtained using two burner arrangements: a 10 mm converging nozzle and a straight tube of 5mm diameter.

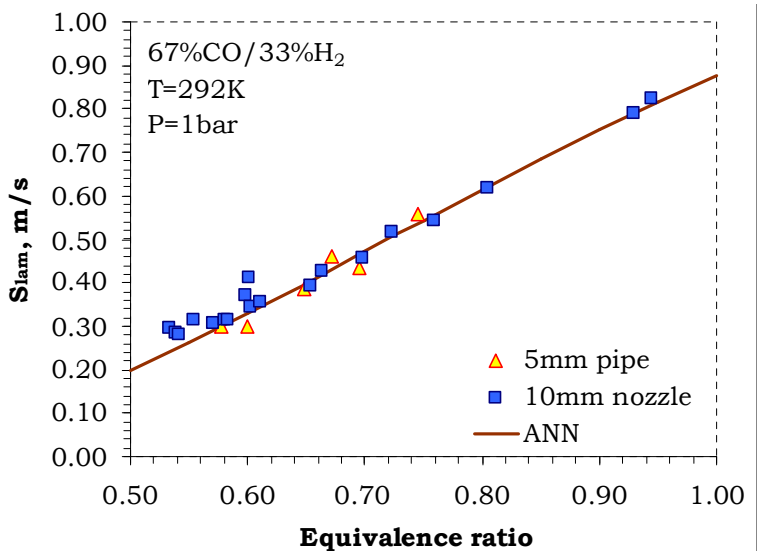

Figure 7: Laminar burning velocities for 67%CO/33%H_2 mixture at ambient conditions obtained with 10mm nozzle and 5mm pipe and compared to artificial neural network

From 7 we see that there is no substantial difference between the laminar burning velocity values obtained with the different burner arrangements for equivalence ratios between 0.6 and 0.75. In addition, experimental values compare well with those obtained from the artificial neural network (ANN). The discrepancy between experimental and numerical data is less than ±4% for the 10mm nozzle. The laminar burning velocity values obtained with the 5mm straight tube are somewhat more scattered but the discrepancies are less ±10%. For leaner flames, with equivalence ratios less than 0.6, the experimental laminar burning velocities are higher and more scattered in comparison with the predictions; the discrepancies approach 20% in some cases.

The motivation behind the change of exit nozzle was that flames at equivalence ratios 0.95 and higher attained irregular and cellular shapes. It was anticipated that hydrodynamic strain introduced by the velocity gradient in fully developed pipe flow would help to reduce these irregularities if they arose from comparatively weak thermo-diffusive processes.

The effect of burner rim cooling

Heat transfer from the flame base to the burner rim was considered to be an additional source of uncertainty in prescribing initial mixture temperature and promoting flashback. An external water-cooled jacket of approximately 1 cm axial extent was therefore mounted close to the rim of the 5mm tube burner to compensate for the local pre-heating.

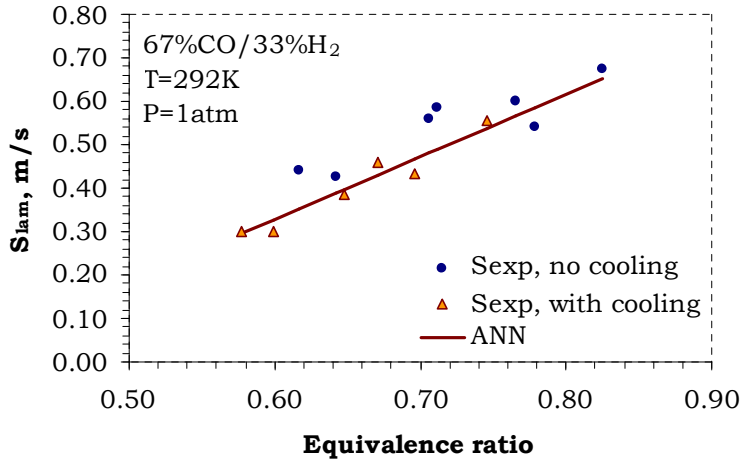

Figure 8: Laminar burning velocities for 67%CO/33%H_2 mixture at ambient conditions for experiment with mounted water cooling jacket and without it

Experiments were performed on the 5mm tube with and without burner rim cooling in order to investigate its effect on measured laminar burning velocity.

The results with both configurations (identified as no [jacket] cooling / with cooling) are presented in Figure 8. From the results it can be seen that the laminar burning velocities with the "no cooling" arrangement are slightly higher in comparison with those with nozzle rim cooling. The laminar burning velocities for the arrangement without cooling are generally under-predicted, consistent with the computations being performed at a lower temperature than realised in practice, given the rim pre-heating. It can be observed that the under-prediction is not entirely systematic; some differences are larger whilst others are comparatively close to the numerical values. This may reflect the fact that some flames were stabilized at slightly higher mass flows than others, resulting in higher hydrodynamic strains and higher heat transfer from the burner rim to the reactants.

One might expect these effects to be reversed as the residence time of the reactants in contact with the nozzle wall is reduced but the velocity increase in the nozzle tube results in higher rates of convective heat transfer even though the residence time is shorter.

Mixture with 50%CO/50%H_2

For this mixture the burning velocities were found to vary from 0.31 m/s to 1.79 m/s over the measured equivalence ratio range, see Figure 9. The experimental laminar burning velocities compare well with numerical predictions; the discrepancy is less than 10%.

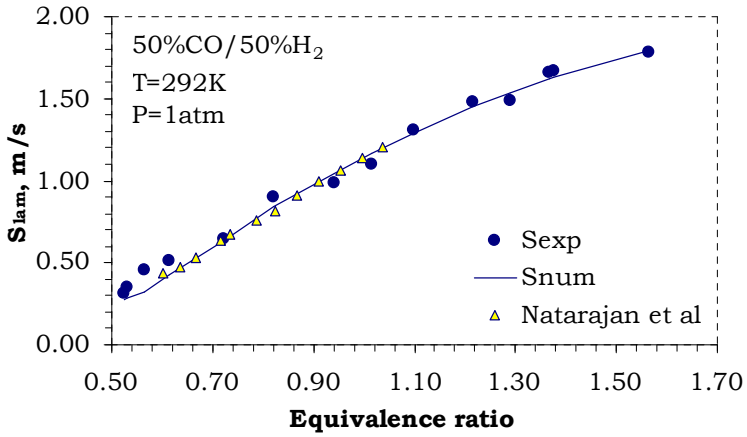

Figure 9: Laminar burning velocities for 50%CO/50%H_2 mixture at ambient conditions

In addition, the measured values obtained in this study compare well with Bunsen burner experiments reported by Natarajan et al [6].

Mixture with 1.5%CO/28.5%H_2/70.0%N_2

The range of burning velocities for this heavily-diluted mixture was found to vary from 0.23 m/s to 0.50 m/s over the more restricted measured range, cf. Figure 10. The experimental laminar burning velocities compare reasonably well with numerical values; the discrepancy is less than 20% (for most data points it is less than 10%).

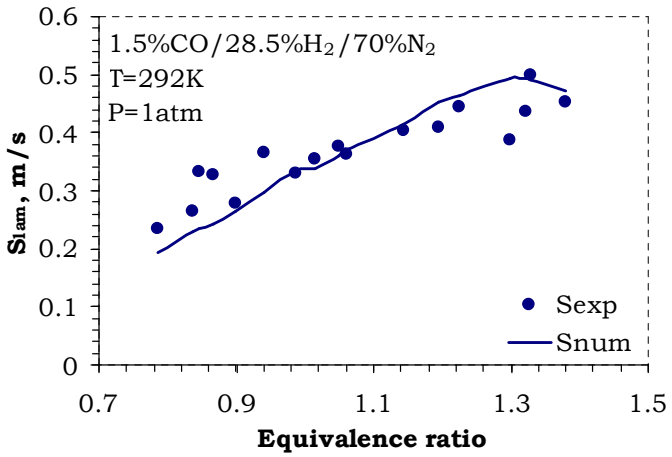

Figure 10: Laminar burning velocities for 1.5%CO/28.5%H_2/70%N_2 mixture at ambient conditions

The discrepancies are larger for leaner flames because these flames do begin to display polyhedral shapes for almost the entire range of equivalence ratios, resulting in greater uncertainty for the flame area calculations. In addition, as discussed in more detail later, the actual mixture composition at the flame front in these distorted flames may be richer than the nominal one.

Mixture with 57%H_2/43%N_2

For this hydrogen-rich mixture the burning velocities vary from 0.28 m/s to 1.22 m/s over the measured equivalence ratio range, see Figure 11. The experimental laminar burning velocities compare reasonably well with numerical values for equivalence ratios higher than 0.6; again, the discrepancy is generally less than 10%. For the flames at lower equivalence ratios, the discrepancy is much larger –

around 50%, with the experimental laminar burning velocities considerably larger than the numerical values.

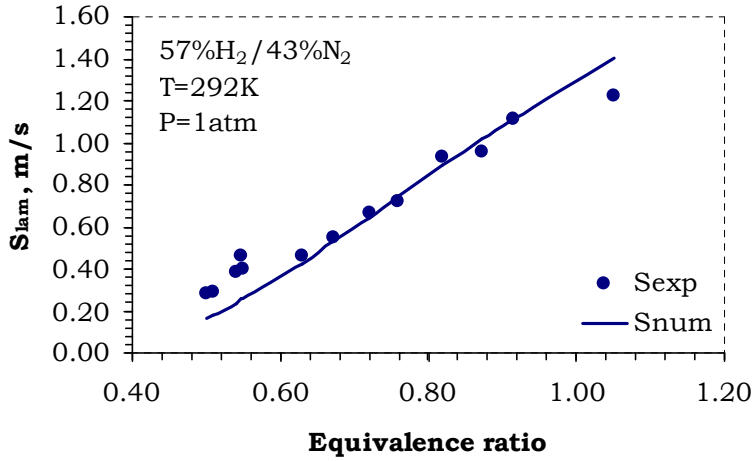

Figure 11: Laminar burning velocities for 57%H_2/43%N_2 mixture at ambient conditions

The burning velocity can be seen peaking at an equivalence ratio of 1.6 for 50%CO/50%H_2 and 1.3 for 1.5%CO/28.5%H_2/70%N_2 respectively, see Figure 9 and Figure 10 The experimental results for 67%CO/33%H_2 and 57%H_2/43%N_2 also indicate that the peak laminar burning velocities should be achieved at equivalence ratios greater than unity; see **Error! Reference source not found.** and Figure 15. This contrasts with the laminar burning velocity trends for hydrocarbon fuel-air mixtures, where the maximum burning velocity is achieved at near stoichiometric concentrations. This displacement to richer mixtures is evident for both H_2 and CO, with that for a pure hydrogen-air mixture laminar burning velocity peaking at equivalence ratio 1.8 [9] at ambient temperature and pressure. The reason for such behaviour is that flame zone reactivity depends not only on the chemical reaction rate within the flame front, but also on the rate of back-diffusion of heat and free radicals from the burned gases to the unburned mixture. This back diffusion is needed to activate the fresh reactant and although the reaction rate for a hydrogen-air stream reaches a maximum at stoichiometric conditions, the maximum effective diffusivity occurs at much higher hydrogen concentrations.

4.2 Effect of Preheat Temperature

In order to investigate the effects of reactant preheat, all the mixtures were examined over the range of temperatures from room temperature to 600K.

As the unburned reactant temperature increases, so the laminar burning velocity also rises. This increase in laminar burning velocity requires operating at a proportionately higher average reactant flow velocity. Fortunately, the flow in the tube remains laminar due to the accompanying increase in mixture viscosity. The 67%CO/33%H_2 tests were performed on the 10mm burner whilst the other three mixtures tests were performed on the 5mm tube burner.

The effect of preheat temperature on the 67%CO/33%H_2 fuel mixture is shown in Figure 12. The measured and computed laminar burning velocities compare well up to a preheat temperature of 443K over the entire range of equivalence ratios measured. As the temperature is increased further, the discrepancy between measured and calculated laminar burning velocities increases, with larger differences for richer mixtures. The computed laminar burning velocities eventually over-predict measured values by as much as 20%.

Similar results were obtained with the 50%CO/50%H_2 fuel mixture composition, cf. Figure 13. As in the 67%CO/33%H_2 case, the computed and measured laminar burning velocities are in good agreement up to 400K. Above this temperature, the discrepancy between computed and experimental values again increases. The computed laminar burning velocities are higher than experimental ones; the discrepancy is around 15%. The data of Natarajan et al [6] exhibit a similar trend.

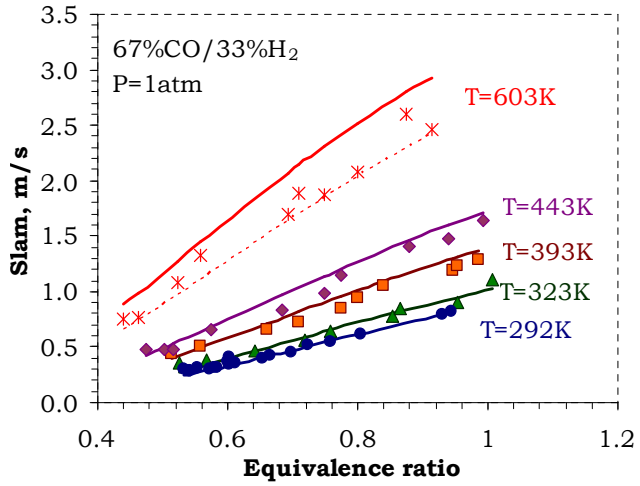

Figure 12: Laminar burning velocities for 67%CO/33%H_2 mixture at various preheat temperatures (10mm converging nozzle); points: experimental results, lines: numerical and dotted line: T-50K

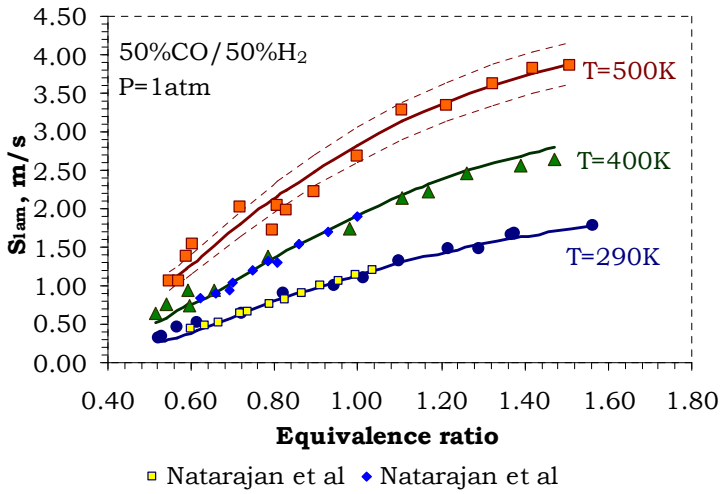

Figure 13: Laminar burning velocities for 50%CO/50%H_2 mixture at various reactant temperatures; points: experimental results, lines: numerical and dotted lines: T±20K

For the fuel mixture with 1.5%CO/28.5%H_2/70%N_2 , the experimental laminar burning velocities again compare well with numerical values at a preheat temperature of 360K; the discrepancy is less than 10%, see Figure 14. For a temperature of 500K, the experimental values are more scattered because the reactant exit temperature was not exactly 500K, but varied between 480K and 525K. The discrepancy between experimental and numerical laminar burning velocities at preheat temperatures of approximately 500K is around 20%.

For the fuel mixture with 57%H_2 and 43%N_2 the discrepancies between experimental and numerical values approach 30% at a preheat temperature of 500K, cf. Figure 15. The computed laminar burning

velocities over-predict the experimental values. As for all other mixtures, at preheat temperatures of 400K, the experimental and numerical values compare very well. The discrepancies are less than 10%.

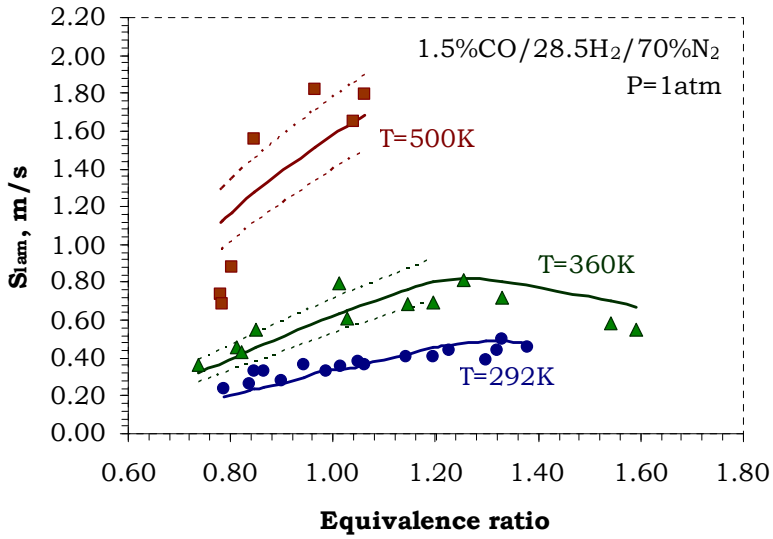

Figure 14: Laminar burning velocities for 1.5%CO/28.5%H_2/70%N_2 mixture at various reactant temperatures; points: experimental results, lines: numerical and dotted lines: T±20K

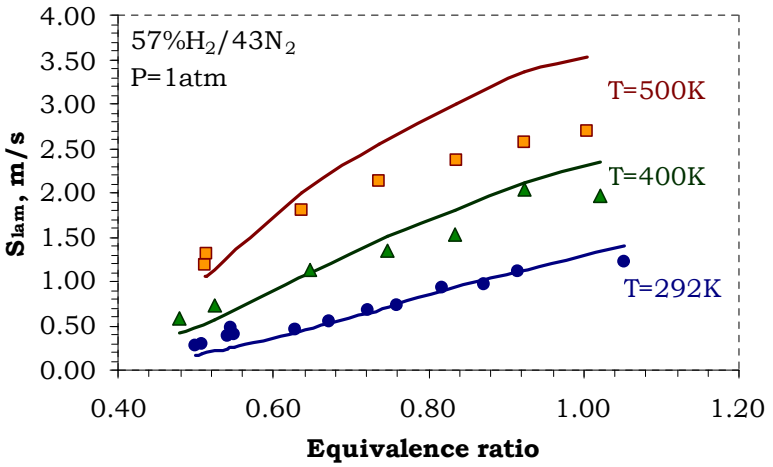

Figure 15: Laminar burning velocities for 57%H_2/43N_2 mixture at various reactant temperatures

Natarajan et al. [6] suggests that the difference between the experimental and numerical predictions of laminar burning velocities at higher preheat temperatures indicates either errors in the temperature dependence of the chemical mechanism or in the mixture transport properties (e.g., diffusivities) used in the computations or systematic errors in the experimental measurements.

The measurements of the reactant preheat temperature are challenging because thermocouple measurements at the burner exit are impractical – the flame stabilises on the thermocouple - and can only be made upstream, remote from the flame, or in the absence of the flame.

The measurement of the exterior burner wall temperature is possible but, arguably, scarcely representative. The thermocouple must be close enough to the burner rim to minimise heat loss to the surroundings – an effect that becomes more significant with increase in reactant preheat temperature. In

addition, however, the measured temperature may be inflated due to heat transfer from the flame to the rim.

4.3 Effect of Pressure

Experiments with all four gas mixtures were performed at higher pressures in order to investigate the pressure effect on laminar burning velocity.

Results for high pressure tests of the gas fuel mixture composed of 33%H_2/67%CO and obtained on the 5mm tube are presented in Figure 16. For this experimental arrangement, stable laminar flames could be acquired for pressures up to 5 bar and for very lean mixtures with equivalence ratios below 0.7. Only very few flames at 6 and 7 bars could be satisfactorily rim stabilised.

In general, it has not proved possible to get data for richer flames because the Re number - even in the 5mm tube - approaches 2000 and the flow enters the transitionally turbulent regime.

Unlike the numerical simulations, these experiments indicate that pressure has comparatively little effect on laminar burning velocities at very lean equivalence ratios. By contrast, numerical predictions suggest that the laminar burning velocity falls by a factor of 2 with increase in pressure from 1 to 3 bar.

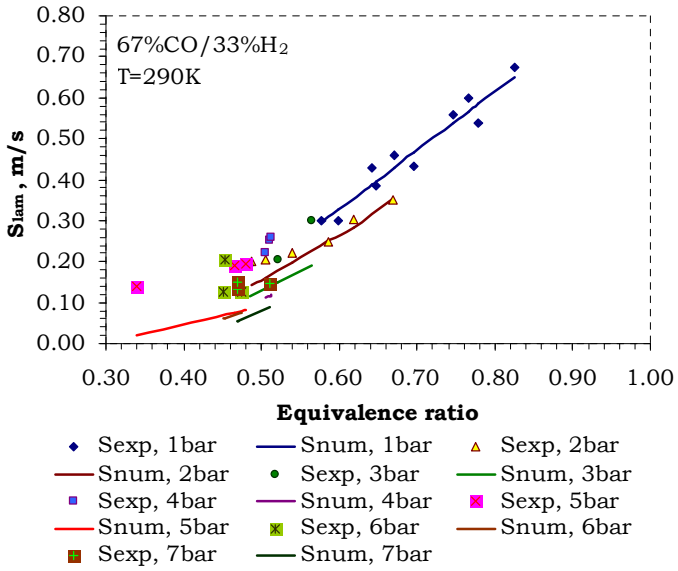

Figure 16: Laminar burning velocities of 33%H_2/67%CO fuel mixture at different pressures

The data are quite scattered, however, and the uncertainties identified affect both the reactant conditions underlying the predictions and the flame shapes.

The results for mixtures with 50%CO/50%H_2, 1.5%CO/28.5%H_2/70%N_2 and 57%H_2/43%N_2 show similar trends. Experimental laminar burning velocities for these mixtures are again over-predicted.

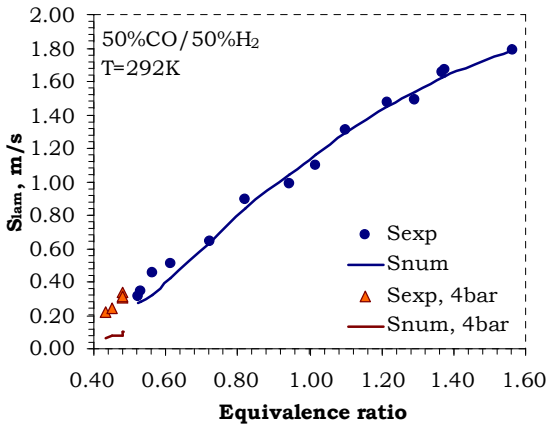

Figure 17: Laminar burning velocities for 50%CO/50%H_2 mixture at ambient and 4bar pressures

For mixture with composition of 50%CO/50%H_2 laminar burning velocities at 4bar pressure were obtained for very lean mixtures with equivalence ratios between 0.43 and 0.48, cf. Figure 17. These equivalence ratios are close to the lean flammability limit. Again it was not possible to stabilise laminar flames for richer mixtures with higher burning velocities, given the onset of turbulent flow. This mixture is more reactive than that of 67%CO/33%H_2; therefore the laminar burning velocities are greater and require higher mass flows to avoid flashback.

For the mixture with 1.5%CO/28.5%H_2/70%N_2 it was possible to get laminar burning velocities for flames at equivalence ratios between 0.64 and 0.9 and reactant temperatures of 292K and 400K, see Figure 18 and Figure 19. From both figures it can be seen that flames were stabilised at broader equivalence ratios region for 400K reactant preheat temperature.

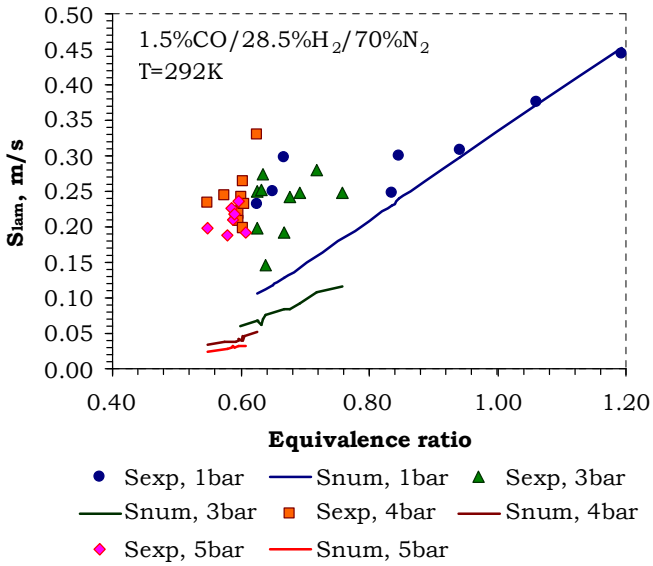

Figure 18: Laminar burning velocities for 1.5%CO/28.5%H_2/70%N_2 mixture at different pressures

By comparison with the other fuels investigated, this mixture is heavily diluted with nitrogen. The laminar burning velocities are therefore much lower and consequently laminar burning velocity data could be obtained at richer equivalence ratios with lower mass flows.

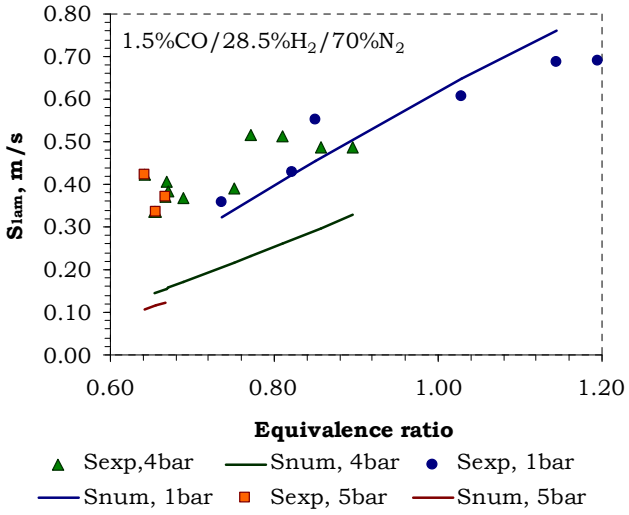

Figure 19: Laminar burning velocities for 1.5%CO/28.5%H_2/70%N_2 mixture at different pressures and T=360K (1bar pressure) and T=400K (4bar and 5bar pressure)

For the mixture with composition of 57%H_2/43%N_2 laminar burning velocities were obtained at 2bar pressure and equivalence ratios between 0.48 and 0.75, cf. Figure 20. These data were obtained only at 500K temperature, because it was not possible to stabilise any laminar flames at ambient temperature and higher pressures for this mixture. Laminar burning velocities are high for this mixture, therefore higher mass flows are needed to avoid flashback and secure stable flames.

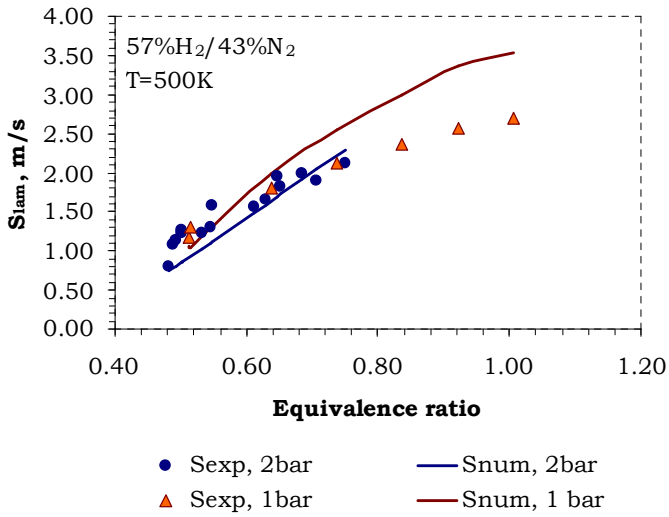

Figure 20: Laminar burning velocities for 57%H_2/43%N_2 mixture at different pressures and 500K temperature

It is possible that the discrepancies between experimental and numerical values can be explained on the basis that the experimental values are reliable and that there are shortcomings in the GRI Mech 3.0 at higher pressures for very lean flames since the mechanism was largely designed and validated to simulate methane combustion under ambient conditions.

Alternatively, it is possible that the actual flame area is substantially under-estimated from the Schlieren images, resulting in an over-estimate of the area-averaged laminar burning velocity. Lean flames at higher pressures do appear increasingly susceptible to cellular disturbance promoted by preferential diffusion.

Another explanation could be that heat is transferred from the flame into rim of the burner due to axial conduction further downstream. Some heat is transferred into the reactant flow raising the gas temperature, while some of it is carried away by the cooling water. As the laminar burning velocities are comparatively low, reactant flow velocity is lower too and the reactant heating effects on laminar burning velocity of lean flames at high pressures are amplified.

4.4 Polyhedral flames

Cellular flame structures, characterised by the formation of cells and ridges over the flame surface having well-defined scales, are recognised phenomena in flame dynamics of long standing [10] and have been widely discussed in premixed flames over the years [1,12]. The basic mechanisms driving cellular flame instabilities, and many other aspects of the flame dynamics, can be explained quite generally [13] in terms of preferential diffusion and hydrodynamic interactions.

In the present investigation, polyhedral flames at ambient pressure were observed in the equivalence ratio range of 0.626 to 0.786 for the fuel mixture 1.5%CO/28.5%H_2/70%N_2; only one flame at equivalence ratio 0.523 for fuel mixture 50%CO/50%H_2 and 0.499 to 0.541 for fuel mixture 57%H_2/43%N_2. No polyhedral flames were observed for the mixture with 67%CO/33%H_2 but nor were systematic efforts made to identify them. The number of sides in the polyhedral structures observed varied from 3 edges at an equivalence ratio of 0.523 (50%CO/50%H_2) to 10 edges at an equivalence ratio of 0.743 (1.5%CO/28.5%H_2/70%N_2). All the high pressure flames displayed some polyhedral features. Schlieren photographs covering all the fuel mixtures are illustrated in fig.21; the number of edges varies from 4 up to 10.

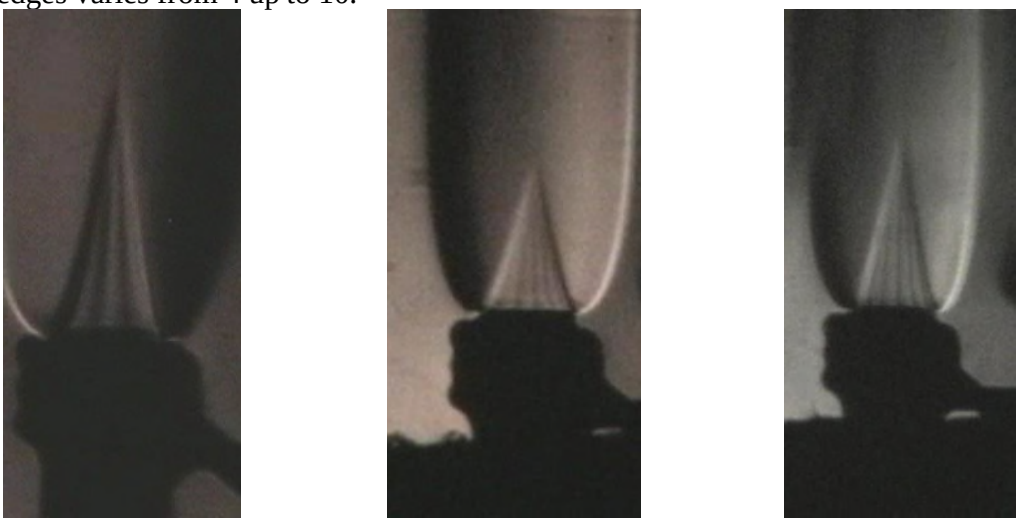

a) b) c)

Figure 21: Polyhedral flames; a) mixture 67%CO/33%H_2 at ϕ=0.522, T=435K, P=3.05bar; b) mixture 50%CO/50%H_2, at ϕ=0.464, T=517K, P=4.29bar, c) mixture 57%H_2/43%N_2 at ϕ=0.521, T=517K, P=2.9bar

In the present experiments, the appearance of polyhedral flames is evidently related to the presence of low molecular weight hydrogen in the fuel mixtures. Large variations in diffusivity accompany both light and heavy fuel components, relative to the predominant species nitrogen. Such flames have previously been observed in lean mixtures of hydrogen-air and in rich mixtures of heavy hydrocarbons-air flames [14].

Different zones of combustion create polyhedral flame surfaces, where, for example, the burning velocity in locally hydrogen-rich zones will be greater than elsewhere.

Weak tip flames

Some weak flames at high pressures with equivalence ratio between 0.55, and 0.97 for fuel mixture 1.5%CO/28.5%H_2/70%N_2 had a tip, which was barely luminous or even completely open. Bunsen burner flame tip opening/weakening is also attributed to the non-equidiffusive mixture (non unity Lewis numbers) along with the presence of a strong stretch at the tip of the flame [10].

The burning intensity of premixed Bunsen flames has been reported to be sensitive to both stretch effects, flame curvature and the preferential diffusion of heat or mass. Mizomoto et al [15, 16] quantified these effects and showed that lean hydrogen-air mixtures have open tips because of the presence of a strong curvature at the tip and Lewis number of less than unity for those mixtures. They also demonstrated the opposite effect (brightening of the tip) for rich hydrogen-air mixtures.

5. Ignition Delay

The emphasis on low emissions, particularly of NO_X, from the industrial gas turbine has focussed primarily on the development of lean-burning premixed combustion systems. The presence of a premixing chamber upstream of the combustor, in turn, emphasises the importance of preventing flashback and autoignition. Whilst the former is largely a matter of aero-thermal design, the latter is strongly influenced by fuel composition and chemical kinetics. Simulations have therefore been performed of ignition delay for the gas mixtures examined here in respect of burning velocity.

The ignition delay time, used to quantify the ignition of a combustible mixture, is defined to be the time interval required for the mixture to spontaneously ignite under prescribed conditions of temperature, pressure and equivalence ratio. The definition of an ignition criterion from conditions in a homogeneous reactor is open to interpretation. We here adopt the convention that the delay is the time elapsed before the reactants in a perfectly-stirred reactor show a 5% temperature rise with respect to the initial conditions. The calculations were performed using the GRI mechanism in CHEMKIN. The characteristic dependencies are illustrated in the following figures drawn from the larger data set reported by Bunkute [17].

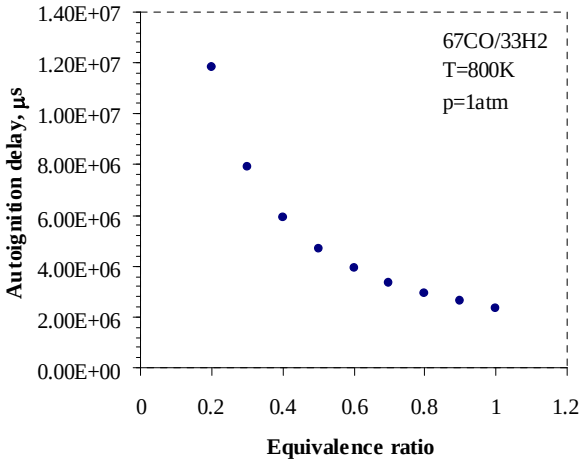

Figure 22: Ignition delay dependence on equivalence ratio for fuel mixture with 67%CO/33%H_2, at 1atm pressure and 1000/T=1.25

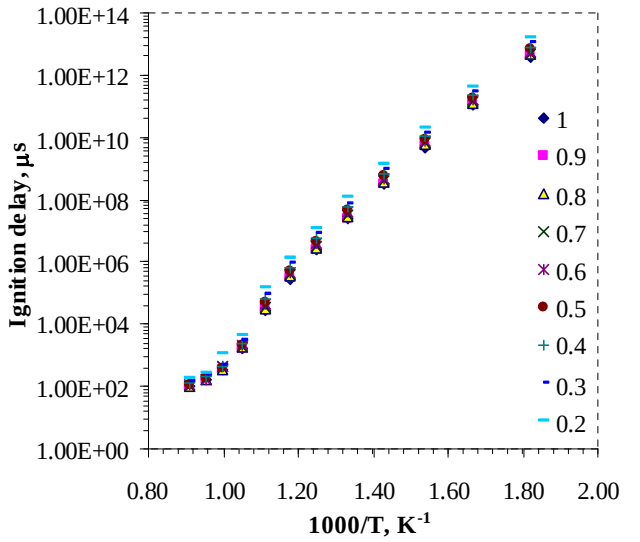

Figure 23: Ignition delay times for fuel mixture 67%CO/33%H2 at 1 atm. and varying temperatures and equivalence ratios

The influence of pressure is such that the ignition delay time for hydrogen-rich mixtures is generally reduced (see Figure 24) but the computations also suggest that this behaviour may be reversed for temperatures in excess of 900K

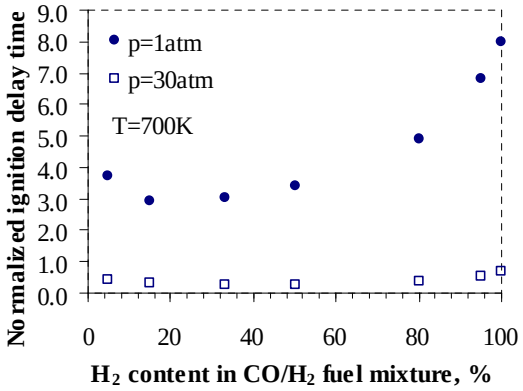

Figure 24: Normalized ignition delay time for various CO/H_2 fuel mixtures at 1atm and 30atm pressures and 700K temperature. [Normalisation factor = 1.0×10^{-8}]

The ignition delay times do exhibit some sensitivity to the reaction mechanism employed. A more detailed discussion of this aspect is to be found in Bunkute [16].

6. Conclusions

Laminar burning velocities for a range of medium and low calorific value gases at different preheat temperatures and pressures have been measured and are presented as functions of equivalence ratio. Experiments were performed on both a converging nozzle and straight tube setups.

Laminar burning velocity values for mixtures with compositions of $67\%CO/33\%H_2$, $50\%CO/50\%H_2$, $57\%H_2/43\%N_2$ and $1.5\%CO/28.5\%H_2/70\%N_2$ are presented. There is generally good agreement between experimental and numerical values at ambient conditions for all mixtures; the discrepancies are less than ±10%. Only for flames at equivalence ratios close to the lean flammability limit are the errors larger.

All mixtures were tested over the temperature range from room temperature to 500K (only for $67\%CO/33\%H_2$ up to 600K) in order to evaluate the effect of reactant preheat on laminar burning velocity. For all mixtures measured laminar burning velocities compare well with computed values for temperatures up to 400K. For higher temperatures the numerical laminar burning velocities over-predict measured values by ~20%.

The flames were confined within a pressure vessel and elevated pressure tests were performed with all mixtures in order to investigate the influence on laminar burning velocity. Data were obtained for very lean flames close to the flammability limit. It was not possible to obtain data for a wider range of richer flames because the Reynolds number of the reactant flow in the tube approaches 2000 and the flow enters the transition-to-turbulent regime. Experimental laminar burning velocity data indicate that the pressure effect on laminar burning velocity is small, though numerical predictions indicate that laminar burning velocity falls by a factor of 2 with pressure rise from 1bar to 3bar. Uncertainties in the experimental arrangement and, in particular, the precise local reactant conditions in the face of heat transfer to the burner, complicate any attempt to attribute the discrepancy solely to shortcomings in the reaction mechanism for lean mixtures at elevated pressure.

Polyhedral flames were seen to form for the weakest fuel mixture 1.5%CO/28.5%H_2/70%N_2 at equivalence ratios < 0.786. All flames at higher pressures for all fuel mixtures exhibited some polyhedral features. The data reported are restricted to those flames with only limited distortion of the flame cone. It was observed, however, that severe stretch at the tip of the premixed cone along with preferential diffusion due to the presence of hydrogen can break the tip open.

Complementary ignition delay data have also been computed for a broadly similar range of fuel compositions and operating conditions. Unlike the calculations for burning velocity, the computed ignition delay times show considerable sensitivity to the details of the underlying chemical mechanism employed.

CFD simulations of a gas turbine combustor are also reported here that demonstrate the application of the syngas burning velocity data in a representative geometry that has been investigated experimentally within a European research programme – albeit only fuelled there with methane. The combustion modelling employed is shown to be both comparatively simple and robust .

7. Future Work

Many synthetic fuel mixtures of practical interest will also contain trace hydrocarbons. The existing burning velocity data set, both experimental and computational, should therefore be extended to include C_1 and C_2 hydrocarbons. Their impact is potentially non-linear and the increased chemical complexity in respect of kinetic mechanisms will need to be carefully assessed computationally.

The application of the approach to a practical combustor burning coal-derived syngas at more representative operating conditions requires further experimental and computational validation.

8. Publications

1. B Bunkute and JB Moss (2007) Laminar Burning Velocities of Carbon Monoxide / Hydrogen – Air Mixtures at High Temperatures and Pressures, Proc. 3rd European Combustion meeting, ECM 2007, Crete.
2. B Bunkute and JB Moss (2007) Combustion Characteristics of Coal-Derived Syngas, Proc. 2007 Int Conf. on Coal Science and Technology, Nottingham.
3. B Bunkute, *Burning Velocities of Coal-derived Syngas Mixtures*, PhD Thesis, Cranfield University, 2007

9. References

[1] FJ Weinberg, *Optics of Flames* , Butterworths, 1963

[2] RJ Kee et al, *CHEMKIN Release 4.0*, Reaction design Inc. San Diego, CA, 2004

[3] DG Goodwin, CANTERA; an open-source extensible software suite for CVD process simulation, *Proc. CVD XVI* (eds. MAllendorf, F Maury and F Teyssandier), Electrochemical Society, 2003

[4] GP Smith, DM Golden, M Frenklach, NW Moriarty, B Eiteener, M Goldenberg, CT Bowman, RK Hanson, S Song, WC Gardiner, VV Lissianski and Z Qin, GRI-Mech 3.0, http://www.me.berkeley.edu/gri_mech/

[5] MATLAB, Neural Networks Toolbox, MathWorks, 2006

[6] J Natarajan, S Nandula, T Lieuwen and J Seitzman, Laminar Flame Speeds of Synthetic Gas fuel Mixtures, *Proc. ASME Turbo Expo* GT2005-68917, 2005

[7] M Zajadatz, G Lauer and W Leuckel, Bestimmung der Brenngeschwindigkeit von typischen mittelkalorischen Brennstoffen fur stationare Gasturbinen, *TURBOFLAM* 3.2.1.6

[8] ANSYS, FLUENT 6.0 Users Manual, 2006
[9] KT Aung, MI Hassan and GM Faeth, Effects of pressure and nitrogen dilution on flame/stretch interactions of laminar premixed H_2/O_2N_2 flames, *Combust.Flame* 112, 1-15, 1998
[10] CK Law and CJ Sung, Structure, aerodynamics and geometry of premixed flamelets, *Prog Energy Combust. Science*26, 459-505,2000
[11] GH Markstein and LM Somers, Cellular flame structure and vibratory flame movement in n-butane-air mixtures, *4th Int Symp on Combustion*, Combustion Institute 527-535,1952
[12] D Durox, Effects of gravity on polyhedral flames, *24th Int Symp on Combustion,* Combustion Institute 197-204, 1992
[13] S Gutman, RL Axelbaum and GI Sivashinsky, On Bunsen burner polyhedral flames, *Combust Science Tech,* 98, 57-70, 1992
[14] H Behrens, Flame instabilities and combustion mechanisms, *4th Int Symp on Combustion,* Combustion Institute, 538-545,1952
[15] M Mizomoto, Y Asaka, S Ikai and CK Law, Effects of preferential diffusion on the burning intensity of curved flames, *20th Int Symp on Combustion*, 1933-1939,1984
[16] M Mizomoto and H Yoshida, Effects of Lewis number on the burning intensity of Bunsen flames, *Combust.Flame* 70, 47-60,1987
[17] B Bunkute, *Burning Velocities of Coal-derived Syngas Mixtures*, PhD Thesis, Cranfield University, 2007

Appendix A – Laminar burning velocities

67%CO/33%H_2

Table A 1: Laminar burning velocities for mixture with 67%CO/33%H_2 at 1atm pressure and different reactant preheat temperatures, m/s

p=1atm												
	Temperature											
ϕ	300K	350K	400K	450K	500K	550K	600K	650K	700K	750K	800K	850K
1	0.911404	1.157564	1.444433	1.784129	2.175313	2.623196	3.148562	3.766254	4.489869	5.414919	6.424127	7.825444
0.95	0.844226	1.078952	1.366479	1.674119	2.043857	2.485415	2.991079	3.581254	4.289941	5.185023	6.176812	7.558642
0.9	0.778145	0.997211	1.259436	1.562536	1.910648	2.338258	2.81017	3.384505	4.079711	4.939784	6.006045	7.269474
0.85	0.712828	0.914097	1.156033	1.441761	1.770453	2.167297	2.638838	3.189467	3.859446	4.676813	5.715984	6.958604
0.8	0.638628	0.825685	1.051891	1.314665	1.630056	2.009291	2.447063	2.96808	3.653066	4.426166	5.405645	6.57676
0.75	0.564845	0.735913	0.939621	1.173667	1.475692	1.832634	2.247879	2.72817	3.384103	4.127264	5.073663	6.293606
0.7	0.492776	0.644956	0.830359	1.060947	1.319323	1.664533	2.033665	2.498539	3.101684	3.81238	4.719397	5.891572
0.65	0.414683	0.553803	0.718776	0.924169	1.15931	1.470056	1.808346	2.24981	2.803482	3.47714	4.342176	5.475127
0.6	0.343422	0.461587	0.605383	0.781685	0.997909	1.26227	1.589599	1.982147	2.490725	3.123258	3.941764	5.02718
0.55	0.277861	0.372982	0.4926	0.646221	0.834443	1.072664	1.36394	1.718804	2.170025	2.775714	3.517395	4.54735
0.5	0.210505	0.289101	0.38989	0.516449	0.674924	0.879189	1.139935	1.437361	1.851947	2.386714	3.119984	4.023677
0.45	0.150991	0.213241	0.292545	0.39361	0.524346	0.689801	0.904097	1.170628	1.518228	1.978681	2.63984	3.56031
0.4	0.098258	0.144144	0.203196	0.280052	0.384113	0.5141	0.677235	0.904751	1.193175	1.61549	2.169066	3.006499
0.35	0.056209	0.086663	0.128657	0.182549	0.252578	0.353332	0.481803	0.664173	0.893616	1.222856	1.681498	2.38731
0.3			0.067246	0.103572	0.153848	0.221339	0.313478	0.44078	0.609361	0.859455	1.245168	1.777901
0.25					0.070269	0.112716	0.172507	0.25726	0.378103	0.54968	0.799604	1.239124
0.2							0.066751	0.116737	0.188588	0.298322	0.467521	0.742704
0.15										0.112671	0.206714	0.36049
0.1												0.106066

Table A 2: Laminar burning velocities for mixture with 67%CO/33%H_2 at 2atm pressure and different reactant preheat temperatures, m/s

P=2atm								
	Temperature							
f	300K	350K	400K	500K	600K	700K	800K	900K
1	0.792048	1.01916	1.280909	1.933108	2.815776	4.011935	5.724216	8.383165
0.9	0.670791	0.865034	1.095334	1.671689	2.462565	3.563928	5.154258	7.760703
0.8	0.53456	0.699079	0.891491	1.376729	2.08429	3.078339	4.539841	6.966556
0.7	0.40257	0.529818	0.684605	1.094374	1.695511	2.541851	3.912946	6.113981
0.6	0.280569	0.368924	0.484025	0.8002	1.289954	1.979467	3.124926	5.118251
0.5	0.155471	0.21463	0.301104	0.519883	0.862659	1.421999	2.325517	3.975123
0.4		0.100119	0.143605	0.268539	0.498775	0.870973	1.527977	2.785422
0.3				0.095599	0.201322	0.406092	0.784557	1.599706
0.25					0.097514	0.224009		
0.2							0.256181	0.632798
0.1								0.084572

Table A 3: Laminar burning velocities for mixture with 67%CO/33%H_2 at 5atm pressure and different reactant preheat temperatures, m/s

P=5atm							
	Temperature						
ϕ	300K	400K	500K	600K	700K	800K	900K
1	0.620776	1.001432	1.520297	2.222866	3.159752	4.527193	6.536538
0.9	0.513782	0.845128	1.280926	1.911596	2.747317	3.96453	5.806241
0.8	0.401378	0.670158	1.044711	1.56868	2.29088	3.350898	4.998941
0.7	0.291345	0.497912	0.798217	1.224587	1.838708	2.722067	4.149168
0.6	0.189504	0.335228	0.564073	0.894334	1.375379	2.097374	3.278898
0.5		0.193787	0.337475	0.566779	0.923256	1.472679	2.394445
0.45			0.235134				
0.4				0.285935	0.51997	0.889213	1.527942
0.35					0.339771		
0.3					0.203084	0.416641	0.796464
0.25						0.222608	
0.2							0.257228

Table A 4: Laminar burning velocities for mixture with 67%CO/33%H_2 at 10atm pressure and different reactant preheat temperatures, m/s

P=10atm							
	Temperature						
ϕ	300K	400K	500K	600K	700K	800K	900K
1	0.486207	0.786735	1.190362	1.7331	2.484286	3.526802	4.991369
0.9	0.400781	0.649731	0.991876	1.462621	2.118094	3.026315	4.326123
0.8	0.303456	0.506527	0.79029	1.185061	1.732481	2.518111	3.649494
0.7	0.214922	0.36925	0.590196	0.905116	1.349333	1.999447	2.948104
0.6	0.129607	0.235951	0.397511	0.63233	0.944654	1.483043	2.246313
0.55		0.179045					
0.5			0.232683	0.377473	0.612762	0.995177	1.568599
0.45			0.147041	0.277303			
0.4				0.179344	0.32646	0.568561	0.955013

0.35						0.389186	
0.3					0.197344		0.454909
0.25							0.263578

Table A 5: Laminar burning velocities for mixture with 67%CO/33%H_2 at 15atm pressure and different reactant preheat temperatures, m/s

P=15atm						
	Temperature					
ϕ	300K	400K	500K	600K	700K	800K
1	0.411236	0.662899	1.007439	1.469405	2.096276	2.950645
0.9	0.330981	0.542552	0.832862	1.226869	1.76639	2.544925
0.8	0.25021	0.41926	0.652847	0.982064	1.430061	2.066751
0.7	0.170441	0.297029	0.47944	0.743914	1.116673	1.616677
0.65	0.129049					
0.6		0.185082	0.320429	0.507438	0.783773	1.181574
0.5			0.162897	0.295639	0.486531	0.778799
0.45				0.204607		
0.4					0.239281	0.425965

Table A 6: Laminar burning velocities for mixture with 67%CO/33%H_2 at 20atm pressure and different reactant preheat temperatures, m/s

P=20atm							
	Temperature						
ϕ	300K	400K	500K	600K	700K	800K	900K
1	0.360221	0.585188	0.88609	1.288392	1.833682	2.574348	3.604645
0.9	0.287755	0.472997	0.730011	1.067417	1.548347	2.186264	3.075931
0.8	0.215163	0.36279	0.565619	0.853617	1.239985	1.780844	2.557029
0.7	0.140026	0.25407	0.411157	0.639529	0.949811	1.397547	2.046164
0.65		0.203813					
0.6			0.269579	0.409271	0.662333	0.998697	1.500811
0.55			0.194319				
0.5				0.241437	0.402978	0.650332	0.991405
0.45				0.162042			
0.4					0.193897	0.350576	0.589634

50%CO/50%H_2

Table A 7: Laminar burning velocities for mixture with 50%CO/50%H_2 at 1atm pressure and different reactant preheat temperatures, m/s

p=1atm						
	Temperature					
ϕ	300K	400K	500K	600K	700K	800K
1	1.060367	1.725401	2.657321	3.909812	5.641476	8.035172
0.9	0.903121	1.495793	2.322723	3.477903	5.126416	7.445133
0.8	0.73982	1.239846	1.963009	3.024332	4.539946	6.763032
0.7	0.567548	0.976288	1.59206	2.50283	3.877785	5.988943
0.6	0.394865	0.705934	1.191717	1.951784	3.120339	5.077775

0.5	0.229947	0.424445	0.794797	1.377581	2.333285	4.018757
0.4	0.097145	0.195506	0.431577	0.819003	1.49201	2.81577
0.3			0.121893	0.30029	0.719763	1.609046
0.2						0.510443

Table A 8: Laminar burning velocities for mixture with 50%CO/50%H_2 at 5atm pressure and different reactant preheat temperatures, m/s

p=5atm						
	Temperature					
ϕ	300K	400K	500K	600K	700K	800K
1	0.746377	1.226332	1.873513	2.794577	4.135243	6.075958
0.9	0.612585	1.004003	1.564743	2.372493	3.537403	5.328229
0.8	0.469605	0.788212	1.260085	1.939233	2.920095	4.484837
0.7	0.332136	0.575076	0.936274	1.472441	2.299292	3.622151
0.6	0.208333	0.385177	0.642637	1.038284	1.662985	2.698742
0.5	0.106925	0.219238	0.388006	0.647855	1.092242	1.835545
0.4	0.028381	0.073591	0.165166	0.323595	0.587561	1.064435
0.3				0.082161		0.46887

Table A 9: Laminar burning velocities for mixture with 50%CO/50%H_2 at 10atm pressure and different reactant preheat temperatures, m/s

p=10atm						
	Temperature					
ϕ	300K	400K	500K	600K	700K	800K
1	0.578988	0.958893	1.468038	2.195486	3.210041	4.694516
0.9	0.467914	0.774559	1.216374	1.833725	2.688417	3.970618
0.8	0.351342	0.589366	0.931509	1.435339	2.170444	3.255398
0.7	0.239163	0.418179	0.682809	1.064693	1.634139	2.520944
0.6	0.142112	0.257853	0.443674	0.72051	1.147457	1.82131
0.5	0.060704	0.129675		0.431585	0.726402	1.183976
0.4	0.014123	0.037883	0.087806	0.186425	0.35114	0.65888
0.3			0.011824	0.038617		0.244057

Table A 10: Laminar burning velocities for mixture with 50%CO/50%H_2 at 15atm pressure and different reactant preheat temperatures, m/s

p=15atm						
	Temperature					
ϕ	300K	400K	500K	600K	700K	800K
1	0.481154	0.792727	1.229341	1.833936	2.700934	3.910016
0.9	0.386483	0.632224	0.984182	1.48122	2.227399	3.281787
0.8	0.280798	0.476742	0.772614	1.155305	1.756067	2.630018
0.7	0.1881	0.331603	0.544876	0.844993	1.296611	1.998558
0.6	0.106287	0.195442	0.340539	0.576276	0.891697	1.411237
0.5		0.09092	0.169206	0.318224	0.538318	0.88825
0.4		0.025297	0.060549	0.132719	0.25766	0.468687
0.3			0.010709	0.029801	0.076959	0.167906
0.2						0.022879

60%H_2/40%N_2

Table A 11: Laminar burning velocities for mixture with 60%CO/40%H_2 at different pressures and reactant preheat temperatures, m/s

P=1atm						
	Temperature					
ϕ	300K	400K	500K	600K	700K	800K
1	1.237869	2.181918	3.500392	5.200136	7.438367	10.41401
0.9	0.985699	1.810335	3.020464	4.680274	6.816653	9.741685
0.8	0.719469	1.384757	2.493857	4.020742	6.081181	8.94164
0.7	0.472057	0.9561	1.855912	3.246586	5.208728	7.989136
0.6	0.262973	0.570242	1.2163	2.376945	4.170326	6.966163
0.5	0.096067	0.2721	0.653239	1.483093	3.057216	5.648166
0.4			0.193776	0.674851	1.794506	3.980467
0.3					0.565035	2.089419

ϕ=0.8	T=500K
P, atm	
1	3.026571
5	1.899614
10	1.091531
15	0.816873
20	0.524126
25	0.357249
30	0.289054
35	0.248397

1.5%CO/28.5%H_2/70%N_2

Table A 12: Laminar burning velocities for mixture with 1.5%CO/28.5%H_2/70%N_2 at 1atm pressure and different reactant preheat temperatures, m/s

p=1atm						
	Temperature					
f	300K	400K	500K	600K	700K	800K
1	0.328035	0.693291	1.433394	2.553215	4.275551	6.511752
0.9	0.192305	0.470754	1.062416	2.080293	3.730401	5.92923
0.8	0.111484	0.293461	0.67484	1.535462	3.097236	5.426065
0.7	0.057046	0.127879	0.396538	1.027009	2.359	4.604241
0.6		0.049883	0.193672	0.595962	1.553931	3.694794
0.5					0.872013	2.526974
0.4						1.385471

Table A 13: Laminar burning velocities for mixture with 1.5%CO/28.5%H_2/70%N_2 at 5atm pressure and different reactant preheat temperatures, m/s

p=5atm						
	Temperature					
	300K	400K	500K	600K	700K	800K
1	0.113287	0.247109	0.547024	1.152891	2.259668	4.277743
0.9	0.064957	0.153761	0.362363	0.784954	1.708866	3.381861
0.8		0.080601	0.209269	0.479777	1.105734	2.379054
0.7			0.102643	0.264711	0.654841	1.639332
0.6				0.107839	0.31274	0.891256
0.5						0.392581

Appendix B – Artificial neural networks

Here the coefficients of input parameters are used to evaluate the summation function Z_i and activation function F_i. These coefficients represent the weights of the summation function of each neuron belonging to the input, hidden and output layers of the trained network. For this purpose three pairs of equations for input layer, seven pairs for hidden layer and one pair for output layer are required. In order to calculate laminar burning velocities for CO/H2/Diluent fuel mixtures the following equations are derived:

Normalized inputs:

$$P = p / 50$$

$$T = T / 1000$$

For CO, H_2, N_2, CO_2 H_2O and O_2 inputs is the fuel/air mixture composition

Input layer:

Z_{11}=-1.5419•P+0.72823•T-8.7768•CO-8.238•H_2-5.7356•N_2-5.7583•CO_2-5.3679•H_2O-5.3596•O_2+3.1442

$F_{11} = 1/\left(1 + e^{-Z_{11}}\right)$

Z_{12}=3.0004•P+0.92666•T-2.406•CO-4.964•H_2-1.9415•N_2-2.2742•CO_2-0.32524•H_2O+1.9723•O_2+0.91288

$F_{12} = 1/\left(1 + e^{-Z_{12}}\right)$

Z_{13}=-3.0463•P-0.81107•T+3.8621•CO+6.7459•H_2+3.1837•N_2+3.3977•CO_2+1.5083•H_2O-0.71706•O_2-2.1791

$F_{13} = 1/\left(1 + e^{-Z_{13}}\right)$

Z_{14}=-3.7329•P-2.9086•T+0.16543•CO-3.1654•H_2-3.2536•N_2-0.92535•CO_2-4.4852•H_2O-6.5899•O_2+6.6618

$F_{14} = 1/\left(1 + e^{-Z_{14}}\right)$

Z_{15}=-1.7986•P+4.6252•T-18.8267•CO+34.0231•H_2-11.6206•N_2-8.6582•CO_2+13.2641•H_2O-13.6324•O_2+10.2073

$F_{15} = 1/\left(1 + e^{-Z_{15}}\right)$

Z_{16}=2.7651•P-2.9829•T-3.8415•CO-6.3554•H_2+4.0314•N_2+6.9603•CO_2+5.4354•H_2O+5.5788•O_2-5.359

$F_{16} = 1/\left(1 + e^{-Z_{16}}\right)$

Z_{17}=-33.2298•P+ 4.5279•T-11.4712•CO-5.2735•H_2-4.5506•N_2-3.1396•CO_2-5.7091•H_2O-7.7953•O_2-1.7709

$F_{17} = 1/\left(1 + e^{-Z_{17}}\right)$

Z_{18}=9.1198•P-7.4015•T-8.8322•CO-15.8638•H_2-16.7313•N_2+75.8954•CO_2-18.9147•H_2O-16.891•O_2+25.8419

$F_{18} = 1/\left(1 + e^{-Z_{18}}\right)$

Hidden layer

Z_{21}=-19.1551•F_{11}-5.2806•F_{12}-6.0412•F_{13}-1.3673•F_{14}-0.32659•F_{15}-6.1441•F_{16}+1.8346•F_{17}-0.71387•F_{18}+9.1822

$F_{21} = 1/\left(1 + e^{-Z_{21}}\right)$

Z_{22}=-31.6029•F_{11}-5.9029•F_{12}-6.7931•F_{13}+1.5415•F_{14}+0.31315•F_{15}-4.1091•F_{16}-278.698•F_{17}-157.4136•F_{18}+163.2701

$F_{22} = 1/\left(1 + e^{-Z_{22}}\right)$

Z_{23}=274.6936•F_{11}-229.4607•F_{12}-133.1854•F_{13}-93.817•F_{14}+286.8663•F_{15}+21.5655•F_{16}-313.624•F_{17}-5.8279•F_{18}-65.5492

$$F_{23} = 1/\left(1 + e^{-Z_{23}}\right)$$

Z_{24}=61.9735•F_{11}-6.1763•F_{12}-4.5528•F_{13}+4.2081•F_{14}+2.2421•F_{15}+24.536•F_{16}-23.984•F_{17}-3.7273•F_{18}-6.3328

$$F_{24} = 1/\left(1 + e^{-Z_{24}}\right)$$

Z_{25}=84.2177•F_{11}+16.9732•F_{12}-32.827•F_{13}+44.7943•F_{14}+25.0778•F_{15}+115.873•F_{16}+0.76088•F_{17}-40.2286•F_{18}-22.3281

$$F_{25} = 1/\left(1 + e^{-Z_{25}}\right)$$

Z_{26}=-27.6876•F_{11}-3.9531•F_{12}-4.375•F_{13}+0.91339•F_{14}+0.17314•F_{15}+3.4935•F_{16}-296.2584•F_{17}-146.7589•F_{18}+150.7343

$$F_{26} = 1/\left(1 + e^{-Z_{26}}\right)$$

Z_{27}=-22.5093•F_{11}-1.6932•F_{12}-1.5573•F_{13}+0.12706•F_{14}+0.04774•F_{15}+3.9699•F_{16}-312.052•F_{17}-132.5845•F_{18}+134.3748

$$F_{27} = 1/\left(1 + e^{-Z_{27}}\right)$$

Z_{28}=1.4976•F_{11}+23.8193•F_{12}+20.0979•F_{13}+1.1026•F_{14}+3.3938•F_{15}-1.4617•F_{16}+137.408•F_{17}-24.3627•F_{18}-6.9321

$$F_{28} = 1/\left(1 + e^{-Z_{28}}\right)$$

Z_{29}=-4.728•F_{11}+1.1155•F_{12}+0.51816•F_{13}-0.25745•F_{14}+0.057771•F_{15}+2.1293•F_{16}+47.7743•F_{17}-6.7257•F_{18}+6.2431

$$F_{29} = 1/\left(1 + e^{-Z_{29}}\right)$$

Z_{210}=17.2472•F_{11}+4.0898•F_{12}+4.9378•F_{13}+1.1996•F_{14}+0.26977•F_{15}+4.265•F_{16}-19.4712•F_{17}+3.1065•F_{18}-10.1718

$$F_{210} = 1/\left(1 + e^{-Z_{210}}\right)$$

Z_{211}=13.9411•F_{11}-2.7478•F_{12}-3.5825•F_{13}+0.74634•F_{14}+0.2054•F_{15}+8.6327•F_{16}+326.6362•F_{17}+113.722•F_{18}-111.0347

$$F_{211} = 1/\left(1 + e^{-Z_{211}}\right)$$

Output layer

Z_{31}=461.0198•F_{21}-150.7013•F_{22}+115.7326•F_{23}-421.9655•F_{24}+1.9392•F_{25}+412.3337•F_{26}-380.0328•F_{27}+19.7135•F_{28}+218.7266•F_{29}+577.3806•F_{210}-119.0919•F_{211}-492.8283

$$F_{31} = 1/\left(1 + e^{-Z_{31}}\right)$$

Laminar burning velocity, dependant on pressure, temperature and equivalence ratio can be calculated from:

$$S_o = F_{31} \times 20$$

The coefficient 10 is used to convert from normalized value to the actual value of the laminar burning velocity.

Appendix C – Illustrative CFD results

In order to demonstrate the application of the combustion properties database to a typical partially premixed combustion model, 3D combustor simulations were performed using the commercial code FLUENT.

The data needed for this model are laminar burning velocities and critical strain rate to extinction. At the present time, FLUENT (by default) provides laminar burning velocity data for only a limited range of largely pure fuels such as H_2 and simple paraffins. By default only a constant value of critical strain rate to extinction is also provided. FLUENT does , however, provide the possibility of supplying these data in the form of User Defined Functions (UDFs)

By way of illustration here, the fuel mixture with 12%CO/88%H2 was chosen because it has a similar stoichiometric air/fuel ratio and calorific value to the methane that fuelled the PRECCINSTA combustor and hence required minimal geometrical change. The following data were provided to FLUENT in a form of a UDF:

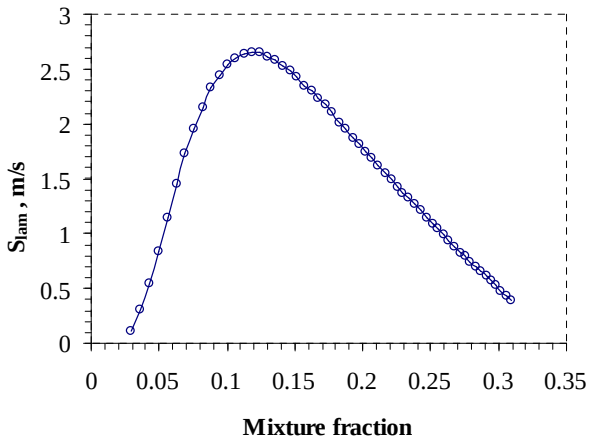

Figure C 1: Laminar burning velocities as a function of mixture fraction

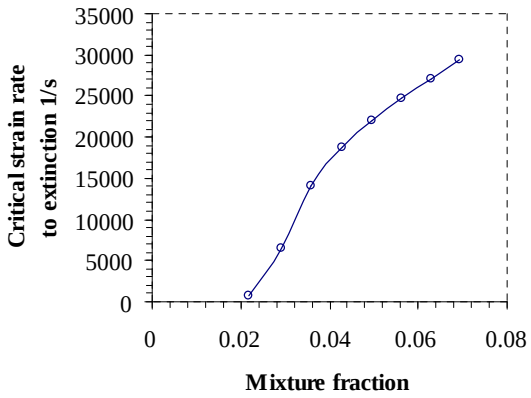

Figure C 2: Critical strain rates to extinction as a function of the mixture fraction

Simulations results plots

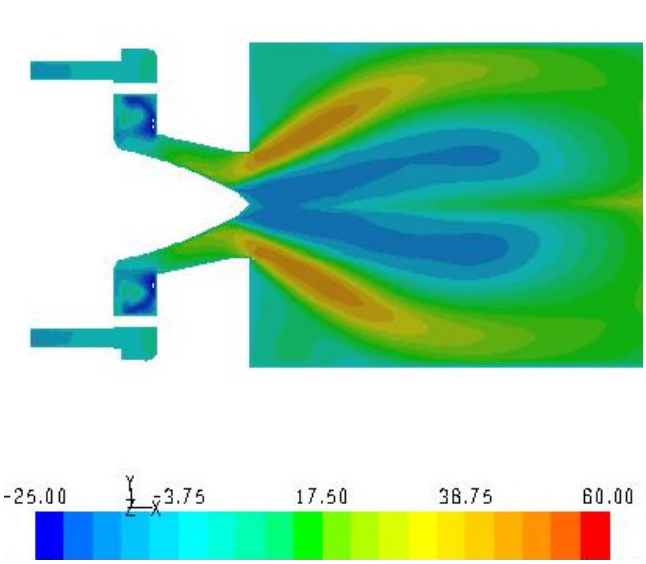

Figure C 3: Axial velocity contours

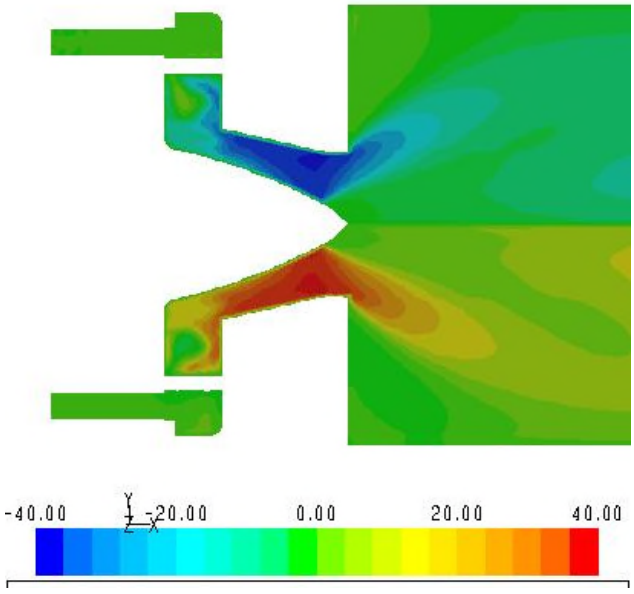

Figure C 4: Tangential velocity contours

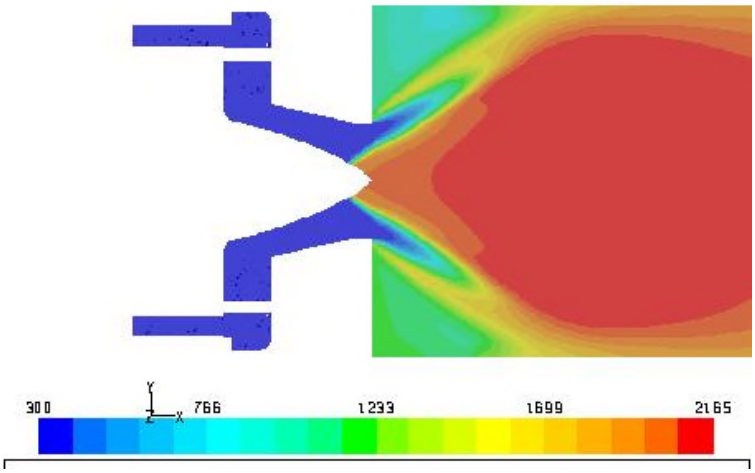

Figure C 5: Temperature contours

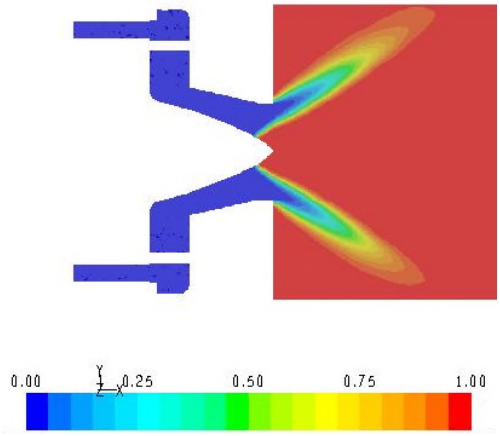

Figure C 6: Progress variable contours, here 0 refers to unburned and 1 to burned

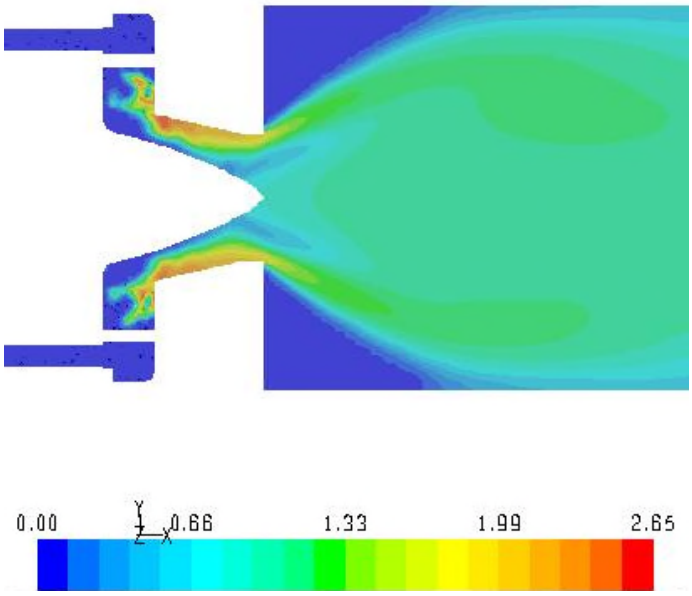

Figure C 7: Laminar burning velocity contours

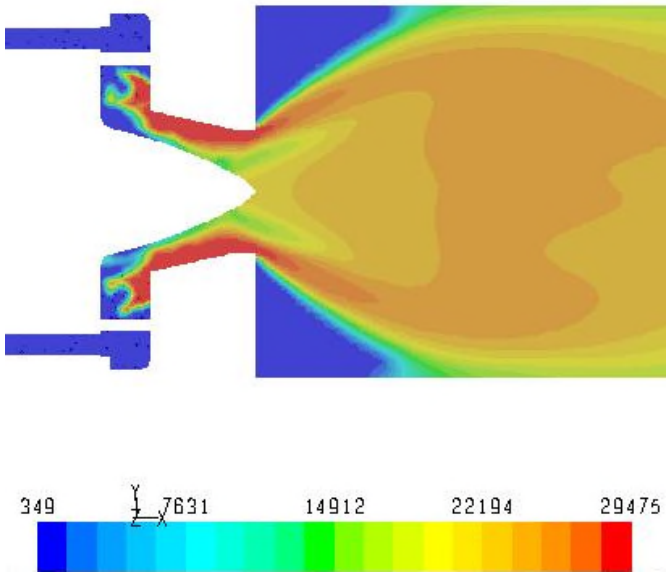

Figure C 8: Critical strain rate to extinction contours

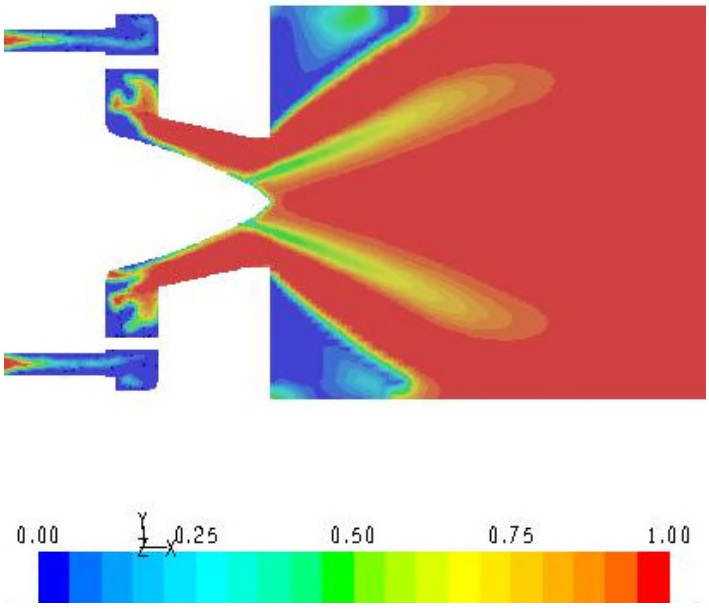

Figure C 9: Stretch coefficient contours

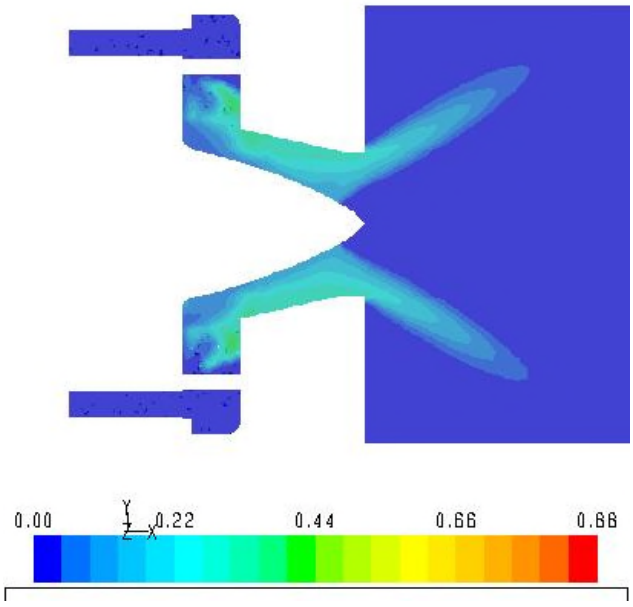

Figure C 10: H_2 mole fraction contours

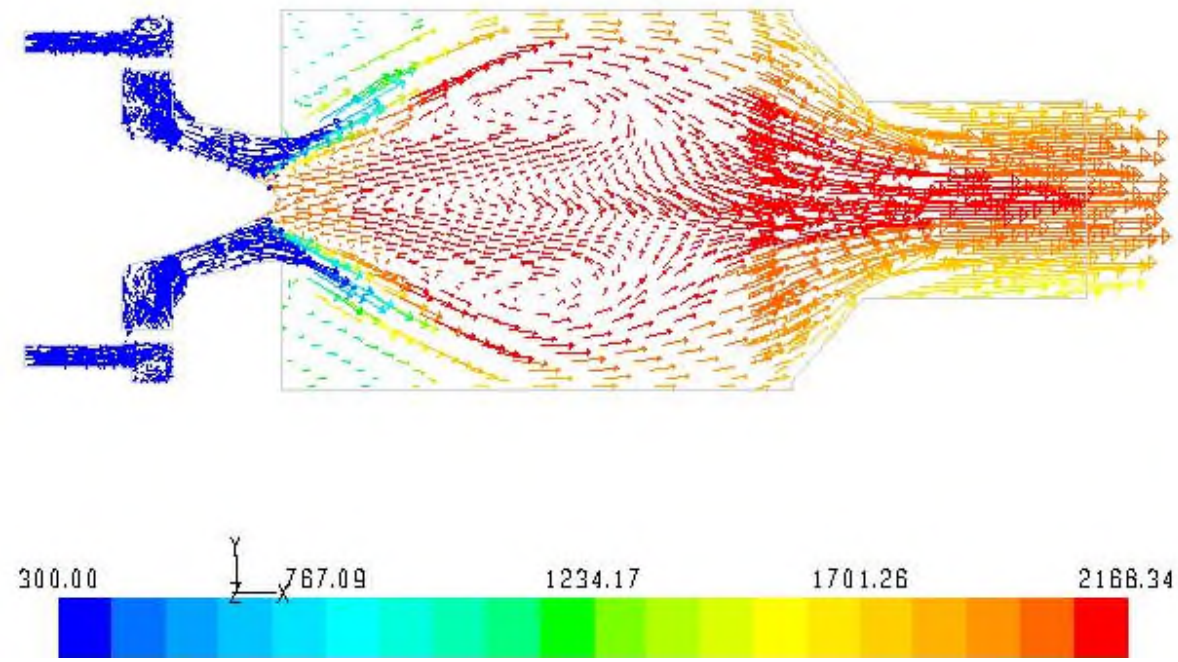

Figure C 11: Velocity vectors colored by temperature

Detailed comparisons of the simulations incorporating the syngas data for differing compositions and flow conditions are reported in [17].